

## ORIGINAL ARTICLE

# Low level of ARID1A contributes to adaptive immune resistance and sensitizes triple-negative breast cancer to immune checkpoint inhibitors

Xin-Yu Chen<sup>1,2</sup> | Bin Li<sup>1,2</sup> | Ye Wang<sup>1,2</sup> | Juan Jin<sup>1,2</sup> | Yu Yang<sup>3</sup> |  
 Lei-Huan Huang<sup>3</sup> | Meng-Di Yang<sup>1,2</sup> | Jian Zhang<sup>1,2</sup> | Bi-Yun Wang<sup>1,2</sup>  |  
 Zhi-Ming Shao<sup>2,4,5</sup> | Ting Ni<sup>3</sup> | Sheng-Lin Huang<sup>2,6</sup> | Xi-Chun Hu<sup>1,2</sup>  |  
 Zhong-Hua Tao<sup>1,2</sup> 

<sup>1</sup>Department of Breast and Urologic Medical Oncology, Fudan University Shanghai Cancer Center, Shanghai, P. R. China

<sup>2</sup>Department of Oncology, Shanghai Medical College, Fudan University, Shanghai, P. R. China

<sup>3</sup>State Key Laboratory of Genetic Engineering, Collaborative Innovation Center of Genetics and Development, Human Phenome Institute, School of Life Sciences, Fudan University, Shanghai, P. R. China

<sup>4</sup>Key Laboratory of Breast Cancer in Shanghai, Department of Breast Surgery, Fudan University Shanghai Cancer Center, Shanghai, P. R. China

<sup>5</sup>Precision Cancer Medicine Center, Fudan University Shanghai Cancer Center, Shanghai, P. R. China

<sup>6</sup>Shanghai Key Laboratory of Medical Epigenetics, International Co-laboratory of Medical Epigenetics and Metabolism, Institutes of Biomedical Sciences, Shanghai Medical College, Fudan University, Shanghai, P. R. China

## Correspondence

Zhong-Hua Tao and Xi-Chun Hu,  
 Department of Breast Cancer and  
 Urologic Medical Oncology, Fudan  
 University Shanghai Cancer Center;  
 Department of Oncology, Shanghai

## Abstract

**Background:** Immune checkpoint inhibitors (ICIs) shed new light on triple-negative breast cancer (TNBC), but only a minority of patients demonstrate response. Therefore, adaptive immune resistance (AIR) needs to be further defined to guide the development of ICI regimens.

**Abbreviations:** AIR, adaptive immune resistance; ARID1A, AT-rich interaction domain 1A; ATAC, Assay for Transposase Accessible Chromatin; ATCC, American Type Culture Collection; Ate, Atezolizumab; BRG1/SMARCA4, SWI/SNF related, matrix associated, actin dependent regulator of chromatin, subfamily a, member 4; ICI, immune checkpoint inhibitor; CCK-8, cell counting kit-8; ChIP, chromatin immunoprecipitation; CN, copy number; CPS, combined positive score; DFS, disease-free survival; DMEM, Dulbecco's Modified Eagle Medium; EGFR, epidermal growth factor receptor; ELISA, enzyme-linked immunosorbent assay; ER, estrogen receptor; FPKM, fragments per kilobase million; FUSCC, Fudan University Shanghai Cancer Center; GB, granzyme B; GEO, Gene Expression Omnibus; GSEA, gene set enrichment analysis; HER2, human epidermal growth factor receptor 2; HR, hazard ratio; HRP, horseradish peroxidase; Hu-PBMC, human peripheral blood mononuclear cell; IFN, interferon; IHC, immunohistochemistry staining; IL, interleukin; ko, knockout; MACS, Model-based Analysis of ChIP-Seq; min, minute; nc, negative control; NPM1, nucleophosmin 1; oe, overexpression; OS, overall survival; PBS, phosphate buffer saline; pCR, pathological complete response; PD-1, programmed cell death-1; PD-L1, programmed cell death 1 ligand-1; PIK3CA, phosphatidylinositol-4,5-bisphosphate 3-kinase catalytic subunit alpha; Pla, placebo; PMA, phorbol 12-myristate 13-acetate; PTEN, phosphatase and tensin homolog; PFS, progression-free survival; RPMI, Roswell Park Memorial Institute; s, second; sgRNA, small guide RNA; shRNA, short hairpin RNA; SWI/SNF, switch/sucrose non-fermentable; TBST, tris buffered saline with Tween-20; TCGA, The Cancer Genome Atlas; TIL, tumor-infiltrating lymphocyte; TIME, tumor immune microenvironment; TMA, tissue microarray; TNBC, triple-negative breast cancer; TPS, tumor proportion score.; UCSC, University of California Santa Cruz.

Xin-Yu Chen and Bin Li contributed equally to this work.

This is an open access article under the terms of the [Creative Commons Attribution-NonCommercial-NoDerivs](https://creativecommons.org/licenses/by-nc-nd/4.0/) License, which permits use and distribution in any medium, provided the original work is properly cited, the use is non-commercial and no modifications or adaptations are made.

© 2023 The Authors. *Cancer Communications* published by John Wiley & Sons Australia, Ltd. on behalf of Sun Yat-sen University Cancer Center.

Medical College, Fudan University, Shanghai 200032, P. R. China.  
Email: drtaozhh@126.com and huxichun2017@163.com

#### Funding information

National Science and Technology Major Project, Grant/Award Number: 2020ZX09201-013

**Methods:** Databases, including The Cancer Genome Atlas, Gene Ontology Resource, University of California Santa Cruz Genome Browser, and Pubmed, were used to screen epigenetic modulators, regulators for CD8<sup>+</sup> T cells, and transcriptional regulators of programmed cell death-ligand 1 (*PD-L1*). Human peripheral blood mononuclear cell (Hu-PBMC) reconstruction mice were adopted for xenograft transplantation. Tumor specimens from a TNBC cohort and the clinical trial CTR20191353 were retrospectively analyzed. RNA-sequencing, Western blotting, qPCR and immunohistochemistry were used to assess gene expression. Coculture assays were performed to evaluate the regulation of TNBC cells on T cells. Chromatin immunoprecipitation and transposase-accessible chromatin sequencing were used to determine chromatin-binding and accessibility.

**Results:** The epigenetic modulator AT-rich interaction domain 1A (*ARID1A*) gene demonstrated the highest expression association with AIR relative to other epigenetic modulators in TNBC patients. Low *ARID1A* expression in TNBC, causing an immunosuppressive microenvironment, promoted AIR and inhibited CD8<sup>+</sup> T cell infiltration and activity through upregulating *PD-L1*. However, *ARID1A* did not directly regulate *PD-L1* expression. We found that *ARID1A* directly bound the promoter of nucleophosmin 1 (*NPM1*) and that low *ARID1A* expression increased *NPM1* chromatin accessibility as well as gene expression, further activating *PD-L1* transcription. In Hu-PBMC mice, atezolizumab demonstrated the potential to reverse *ARID1A* deficiency-induced AIR in TNBC by reducing tumor malignancy and activating anti-tumor immunity. In CTR20191353, *ARID1A*-low patients derived more benefit from pucotenlimab compared to *ARID1A*-high patients.

**Conclusions:** In AIR epigenetics, low *ARID1A* expression in TNBC contributed to AIR via the *ARID1A/NPM1/PD-L1* axis, leading to poor outcome but sensitivity to ICI treatment.

#### KEYWORDS

adaptive immune resistance, *ARID1A*, CD8<sup>+</sup> T cell, *PD-L1*, triple-negative breast cancer

## 1 | BACKGROUND

Adaptive immune resistance (AIR) is crucial for cancer cells to evade immune attack, leading to tumor growth and metastasis. Triple-negative breast cancer (TNBC) comprises 15%-20% of newly diagnosed breast cancer cases and is still the molecular type with the poorest prognosis [1]. Recent studies highlighted the role of AIR in TNBC early metastasis and led to the successful development of immune checkpoint inhibitors (ICIs) targeting programmed cell death 1 (PD-1) and its ligand 1 (PD-L1), alleviating immune suppression and boosting the anti-tumor effect of T cells [2, 3]. Pembrolizumab, an ICI targeting PD-1, has been indicated for early and first-line metastatic TNBC with promising clinical data [4, 5]. Despite the progress, the agent failed to bring survival ben-

efits to most metastatic TNBC patients and heavily treated patients, suggesting the complexity of AIR in TNBC [5–7]. Therefore, we need to integrate a holistic view of the TNBC ecosystem, focusing on AIR in the era of ICIs, and identify biomarkers to improve ICI treatment efficacy.

AIR is under the regulation of both genetic and epigenetic factors. From the genetic perspective, single-gene alterations have been found to alter the immune landscape. Tumor protein p53 mutations, for instance, could suppress innate immune signaling and promote immune evasion [8], whereas deficiency of BRCA2 DNA repair associated was associated with both innate and adaptive immune gene signatures [9]. In recent years, increasing studies have focused on the dynamic role of epigenetic factors such as the innate microenvironment, immune modulation [10] and drug exposure [11]. Recent studies uncovered

a novel role for the mammalian chromatin remodeling complex switch/sucrose non-fermentable (SWI/SNF), a macromolecular assembly repositioning nucleosomes and manipulating DNA accessibility, in regulating anti-tumor immunity and implied therapeutic vulnerabilities underlying aberrations in SWI/SNF core members, such as the AT-rich interaction domain 1A gene (*ARID1A*) [12–14].

As one of the 4 core subunits of SWI/SNF, *ARID1A* has been recognized as a tumor suppressor, and its deficiency was related with poor clinical outcomes across multiple cancer types, including breast cancer [15–18]. In tumors, *ARID1A* alterations, reaching an approximate proportion of 10%, are mostly inactive mutations leading to loss of *ARID1A* protein and inability to direct SWI/SNF to target gene promoters, thereby endowing cells with cancerous functions and causing poor prognosis across multiple cancer types [15, 16, 19, 20]. However, certain exceptions have also been reported. In liver cancer, *ARID1A* demonstrated context-dependent tumor-suppressive and oncogenic roles [21]. In TCGA pan-cancer studies queried in cBioPortal, an *ARID1A*-mutant cohort demonstrated a more favorable prognosis than its *ARID1A*-wildtype counterpart [22]. Therefore, whether *ARID1A* functioned as a friend or foe in TNBC is still worth exploring.

Our previous results in metastatic TNBC patients demonstrated that *ARID1A* was a commonly mutated gene with a rate of 7.1% [23], much higher than that in early TNBC [24]. This trend is consistent with findings in matched primary and metastatic estrogen receptor positive (ER+) breast cancer (3.3% vs. 12.9%,  $P < 0.001$ ) [25]. In heavily treated TNBC patients harboring *ARID1A* mutations, we also observed a better response to anti-PD-1 therapy compared with *ARID1A* wildtype counterparts (data unpublished). Therefore, we reasonably hypothesized that *ARID1A* deficiency could induce AIR and predict a better response to ICI treatment relative to *ARID1A*-proficient TNBC. However, the exact association between *ARID1A* and AIR in TNBC, as well as the underlying mechanisms, remains to be explored.

In the present study, we evaluated the role of *ARID1A* among a series of epigenetic modulators in TNBC and explored how low *ARID1A* expression contributed to AIR. In addition, we assessed the targetability of low *ARID1A* expression-promoted AIR by ICIs.

## 2 | MATERIALS AND METHODS

### 2.1 | Cell culture and reagents

Most cell lines were obtained from American Type Culture Collection (ATCC, Manassas, VA, USA), while human primary T cells were obtained from OriBiotech (Shanghai,

China). All cell lines were authenticated via short tandem repeat genotyping in November 2021. Human TNBC cell line MDA-MB-231 and human embryonic kidney cell line HEK293T were grown in Dulbecco's Modified Eagle Medium (DMEM, Invitrogen, Carlsbad, CA, USA). Human T-cell leukemia cell line Jurkat, human primary T cells and mouse TNBC cell line 4T1 were cultured with Roswell Park Memorial Institute (RPMI)-1640 (Invitrogen), and human TNBC cell line MDA-MB-468 was cultured with Leibovitz's L-15 (Gibco, Grand Island, NY, USA). All media were supplemented with 10% fetal bovine serum (Invitrogen), 100 U/mL penicillin and 100  $\mu\text{g}/\text{mL}$  streptomycin (Invitrogen). MDA-MB-231, HEK293T, Jurkat, human primary T cells and 4T1 cells were cultured in a humidified atmosphere of 5%  $\text{CO}_2$  at 37°C, while MDA-MB-468 cells were cultured under the same conditions except for a  $\text{CO}_2$  concentration of 0.03%.

### 2.2 | Stable transfection using lentiviral infection

To knockout (ko) *ARID1A* through CRISPR/Cas9, the Lenti-CAS9-Puro vector and the GV371-EGFP vector (Shanghai Genechem, Shanghai, China) were sequentially transfected. The latter carried the small guide RNA (sgRNA) sequence, 5'-CACCGATGGTCATCGGGTACCGCTG-3' or 5'-CACCGCCCCTCAATGACCTCCAGTA-3' for *ARID1A* knockout, and 5'-CGCTTCCGCGGC CCGTTCAA-3' for negative control (nc). For *ARID1A* overexpression (oe) using CRISPR/Cas9, a synergistic activation mediator vector (Genechem) was applied which carried the sgRNA sequence 5'-CACCGGGCGCTCTAGC CGCTCAGTC-3' or 5'-CACCGCTTGGGTTCGAGGCTGCT GCG-3', and the empty vector was used as negative control. The GV654 vector (Genechem) was used to clone the short hairpin RNAs (shRNAs) for knocking down *PD-L1* and nucleophosmin 1 (*NPM1*). The sequences of sh*PD-L1* and sh*NPM1* were 5'-CCGGACCATC AAGTCTGAGTGGTACTCGAGTACCACTCAGGACTTG ATGGTTTTTTG-3' and 5'-CCGGCTGGAGGTGGTAGCA AGGTTCCCTCGAGGAACCTTGCTACCACCTCCAGTTTT TG-3', respectively, and the empty vector was used as negative control. The GV657 vector (Genechem) was used to clone the coding sequence of *PD-L1* for overexpression, and the empty vector was used as negative control. The plasmids were transfected into HEK293T cells with Lipofectamine 3000 transfection reagent (L3000-150, Invitrogen), and the virus-containing supernatant was collected 72 h after the incubation. The virus was then concentrated and transfected into TNBC cells with polybrene (sc-134220, Santa Cruz Biotechnology, Dallas, TX,

USA). The transfected cells were selected 2 days later with neomycin for at least 1 week.

## 2.3 | Western blotting analysis

Cells were harvested, and protein was extracted using radio immunoprecipitation assay lysis buffer (PC101, Shanghai Epizyme Biomedical Technology, Shanghai, China). A nitrocellulose membrane (Bio-Rad Laboratories, Hercules, CA, USA) was used to transfer protein, which was incubated for 1 h at room temperature with nonfat milk. Primary antibodies included ARID1A (1:1,000, 12354, Cell Signaling Technology, Danvers, MA, USA), PD-L1 (1:1,000, 13684, Cell Signaling Technology), NPM1 (1:1,000, FC-61991, Invitrogen) and  $\beta$ -Actin (1:1,000, 3700, Cell Signaling Technology). After three washes with tris buffered saline with Tween-20 (TBST, PS103, Shanghai Epizyme Biomedical Technology), the membrane was incubated with an IRDye800-labelled secondary antibody (1:1,000, ab216773, Abcam, Cambridge, UK) for 1 h at room temperature. The blots were developed with an Odyssey CLx Imager (Li-Cor GmbH, Homburg, Germany) and quantified through Image Studio, version 5 (Li-Cor GmbH).

## 2.4 | RNA extraction and real-time quantitative PCR (qPCR) assay

Total RNA was extracted from MDA-MB-231, MDA-MB-468 and 4T1 cells by TRIzol reagent (Invitrogen) according to the manufacturer's instructions. RNA was reversely transcribed and subjected to real-time PCR with SYBR Premix Ex Taq (RR420Q/A/B, TaKaRa Biotechnology Dalian, Dalian, Shandong, China). Thermal cycling was as follows: 94°C for 30 s; 35 cycles of 94°C for 30 s, 55°C for 30 s and 72°C for 30 s; 72°C for 10 min; hold at 4°C. The expression levels were normalized to  $\beta$ -Actin and calculated using the  $2^{-\Delta\Delta Ct}$  method. The primer sequences (5'-3') were as follows:

ARID1A-forward: CCAGCAGAACTCTCACGACC;  
ARID1A-reverse: CTGAGCGAAGGACGAAGACG;  
PD-L1-forward: TGGCATTGCTGAACGCATTT;  
PD-L1-reverse: TGCAGCCAGGTCTAATTGTTTT;  
NPM1-forward: GGAGGTGGTAGCAAGGTTCC;  
NPM1-reverse: TTCCTGGCGCTTTTCTTCA;  
 $\beta$ -Actin-forward: GCACAGAGCCTCGCCTT;  
 $\beta$ -Actin-reverse: GTTGTCGACGACGAGCG.

## 2.5 | RNA-seq library construction and analysis

Total RNA (1  $\mu$ g per sample) was extracted from MDA-MB-231 cells. RNA-seq libraries were prepared using a VAHTS Stranded mRNA-seq Library Prep Kit for Illumina V2 (NR612-01, Vazyme, Nanjing, Jiangsu, China) according to the manufacturer's instructions and sequenced after quality inspection by the Illumina sequencing platform (Illumina, San Diego, CA, USA) on a 150 bp paired-end run. Sequencing reads were processed through FastQC (<http://www.bioinformatics.babraham.ac.uk/projects/fastqc>), and the 3' end 60 nt was trimmed off to remove low-quality nucleotide and adaptor sequences originated from the running off of relatively short inserted fragments. The clean reads were aligned using the spliced read aligner HISAT2 (<http://daehwankimlab.github.io/hisat2/>), which was supplied with the Ensembl human genome assembly (Genome Reference Consortium GRCh38) as the reference genome. Gene expression levels were calculated by fragments per kilobase million (FPKM).

## 2.6 | Analysis of PD-L1 expression on cell surface

MDA-MB-231 and MDA-MB-468 cells were digested into single cells and washed three times with cold phosphate buffer saline (PBS, Gibco). Cells were then resuspended with 100  $\mu$ L PBS and incubated for 15 min on ice with CD274-PE (1:20, 12-5983-42, eBioscience, San Diego, CA, USA) or mouse IgG1 kappa isotype control-PE (1:20, 12-4714-82, eBioscience). After washing with cold PBS, PD-L1 expression on the cell surface was detected by flow cytometry (Thermo Fisher, Boston, MA, USA).

## 2.7 | Cell Counting Kit-8 (CCK-8) and colony formation assay

For CCK-8 cell proliferation assay, cells were seeded in 96-well plates (3,000 cells/well). The absorbance at 450 nm was determined using a microplate reader 2 h after adding 10  $\mu$ L CCK-8 solution (HY-K0301, MedChemExpress, Shanghai, China) to each well. For colony formation assay, cells were seeded in 6-well plates (1,000 cells/well) and cultured for 10-14 days. Colonies were fixed and stained with 0.2% crystal violet. A colony was defined as more than 10 cells, and colonies were counted under the microscope.

## 2.8 | Jurkat coculture and enzyme-linked immunosorbent assay (ELISA) for interleukin (IL)-2

MDA-MB-231 and MDA-MB-468 cells were treated with interferon (IFN)- $\gamma$  (300-02, Peprotech, Rocky Hill, NJ, USA), and Jurkat cells were stimulated with 50 ng/L phorbol 12-myristate 13-acetate (PMA, P8139, Sigma-Aldrich, Saint Louis, MO, USA) and 1  $\mu$ g/mL ionomycin (I3909, Sigma-Aldrich), both for 24 h. Next,  $1 \times 10^4$  TNBC cells/well were seeded in 96-well plates. The supernatants were removed after the cells adhered, and Jurkat cells were added to TNBC cells at a ratio of 4:1 in 200  $\mu$ L media. At 48 h later, the supernatants were collected and examined with a Human IL-2 Valukine ELISA kit (VAL110, Novus, Littleton, CO, USA). The results were analyzed by ELISACalc V0.1 (Shanghai Bluegene Biotech Co. Ltd, Shanghai, China).

## 2.9 | Primary T cell coculture and IFN- $\gamma$ production assay

MDA-MB-231 and MDA-MB-468 cells were treated with IFN- $\gamma$ , and primary T cells were stimulated with 50 ng/L PMA and 1  $\mu$ g/mL ionomycin for 24 h. Next,  $2 \times 10^4$  TNBC cells/well were seeded in 24-well plates. After the cells adhered, the supernatants were removed, and primary T cells were added to TNBC cells at a ratio of 30:1 in 500  $\mu$ L media. At 24 h later, primary T cells were collected, treated with protein transport inhibitor cocktail (00-4980-93, eBioscience) for 6 h, fixed and permeabilized with intracellular fixation and permeabilization buffer set (88-8824-00, eBioscience). Samples were further incubated with IFN- $\gamma$  antibody (1:20, 17-7319-41, eBioscience) for 30 min and analyzed with flow cytometry. Data were assessed using CytExpert (2.2.0.97) [26–29].

## 2.10 | Chromatin immunoprecipitation (ChIP)-qPCR assay

ChIP assay was conducted using SimpleChIP Enzymatic Chromatin IP kit (9002S, Cell Signaling Technology) according to the manufacturer's instructions. In brief, TNBC cells were cultured to approximately  $1 \times 10^7$  and cross-linked by 1% formaldehyde. Chromatin was digested with micrococcal nuclease (10011, Cell Signaling Technology), and the nuclear membrane was broken through several pulses. The DNA fragment length was between 150–900 bp. Chromatin was immunoprecipitated by either control IgG, H3K4me3 (1:50, 9751, Cell Signaling Technology), H3K4me1 (2  $\mu$ g, ab8895, Abcam), H3K27ac (1  $\mu$ g,

C15210016, Diagenode, New Jersey, USA), ARID1A (1:100), SWI/SNF-related, matrix-associated, actin-dependent regulator of chromatin, subfamily A, member 4 (SMARCA4, also known as BRG1) (1:50, 49360, Cell Signaling Technology), or NPM1 primary antibody (1:50, 4TOU-1B2, Invitrogen) and reversely cross-linked. The eluted DNAs were processed by a QIAseq ultralow input library kit (180495, QIAGEN, Nordrhein-Westfalen, German) and quantified by qPCR. Thermal cycling was as follows: 94°C for 30 s; 35 cycles of 94°C for 30 s, 55°C for 30 s and 72°C for 30 s; 72°C for 10 min; hold at 4°C. The primer sequences (5'-3') were as follows:

*PD-L1*-forward-1: TTGGGCCCATTCCTACTAATCCC;  
*PD-L1*-reverse-1: AAGAACTTCCCATCCCGAGC;  
*PD-L1*-forward-2: CTAGAAGTTCAGCGCGGGAT;  
*PD-L1*-reverse-2: GGCTGCGGAAGCCTATTCTA;  
*NPM1*-forward-1: GGTCTTCAGAACGCCCAAT;  
*NPM1*-reverse-1: GGGAGCGAGCATGGGAATTA;  
*NPM1*-forward-2: ACGTTAATCCCATGCTCGC;  
*NPM1*-reverse-2: GGGCCGACTCTGACTTCTTG;  
 F-box protein 38 (*FBXO38*)-forward:  
 GCATGGCGCTTTAGTGTCAG;  
*FBXO38*-reverse: GCCTCAAACCCGTGTCCATA;  
 Nonspecific primer (NSP)-forward: GGAGTGTCACATCTGACCT;  
 NSP-reverse: TCTTCTCGCAGGACACGTCA.

## 2.11 | ChIP-PCR

The immunoprecipitated DNA prepared as above was quantified by PCR amplification with Taq DNA polymerase (Yeasen Biotech, Shanghai, China). PCR primers were the same as those for ChIP-qPCR. Thermal cycling was as follows: 94°C for 30 s; 30–40 cycles of 94°C for 30 s, 52–58°C for 30 s and 72°C for 30 s; 72°C for 10 min; hold at 4°C. The PCR product was visualized in a 2% agarose gel stained with ethidium bromide dye. Values were normalized to input DNA and performed in technical triplicate.

## 2.12 | ChIP-seq library construction and analysis

The DNA fragments obtained as described above were used for library construction following the manufacturer's instructions. Samples were sequenced in Cloud-seq (Shanghai, China) by NovaSeq 6000 (Illumina) after quality inspection, and paired-end reads of 150 nt length were obtained. After the evaluation and cleaning described as above, sequencing reads were aligned to the human

genome (UCSC hg19) with bowtie2 (v2.2.4) [30]. In addition, Model-based Analysis of ChIP-Seq (MACS, v1.4.3) was used for peak calling, and diffReps was applied to find significantly different peak distributions between *ARID1A*-ko and negative control samples [31, 32].

### 2.13 | Dual-luciferase reporter assay

MDA-MB-231 cells were seeded in 24-well plates at  $1 \times 10^5$  cells/well and transfected with 0.5  $\mu\text{g}$ /well luciferase reporter plasmids (Genechem). The cells were cotransfected with 10 ng of pRL-CMV (Renilla luciferase, E2261, Promega, Madison, WI, USA) for normalization. At 48 h post transfection, the luciferase activity was detected using a Dual-Luciferase Reporter Assay System Kit (E1910, Promega) following the manufacturer's instructions.

### 2.14 | Assay for transposase accessible chromatin (ATAC)-seq library construction and analysis

MDA-MB-231 cells were collected and prepared for ATAC-seq analysis as previously described [33]. In brief,  $5 \times 10^4$  cells were washed with PBS and lysed in lysis buffer (10 mmol/L Tris-HCl pH 7.4, 10 mmol/L NaCl, 3 mmol/L  $\text{MgCl}_2$ , 0.1% Nonidet P-40). After centrifugation at  $800 \times g$ ,  $4^\circ\text{C}$  for 15 min, the pellets were resuspended and incubated in a transposition mix containing Tn5 transposase (Illumina) for 30 min at  $37^\circ\text{C}$ . The purified DNA was subsequently ligated with adapters and amplified for 11 cycles. The libraries were purified using AMPure beads (A63882, Beckman Coulter, Hebron, KY, USA) and sequenced on Illumina X-Ten system through a 150 bp paired-end strategy. For data analysis, Trimmomatic (v0.36, <http://www.usadellab.org/cms/?page=trimmomatic>) was used to trim Illumina adapters and reads of low quality. Total reads in each sample were aligned to human reference genome hg19 using bwa (v0.7.11, <https://sourceforge.net/projects/bwa/files/>) with default settings. Samtools (v1.6, <https://samtools.sourceforge.net>) was used to remove low-quality reads (mapping quality  $\geq 20$ ) and reads mapping to mitochondrial DNA, and Picard Tools (v1.4.5, <https://broadinstitute.github.io/picard/>) was used to exclude duplicates. All mapped reads were offset by +4 bp for the positive strand and -5 bp for the negative strand using bedtools (v2.25.0, <https://github.com/arq5x/bedtools2>). Libraries of the same cell lines were merged for subsequent analyses. MACS2 (v2.1.1.20160309, <https://pypi.org/project/MACS2/>) with parameter “-nomodel -shift 100 -extsize 200” was used for peak calling. Peaks with  $P < 0.01$  were merged for searching differential

peaks. Peak annotation and motif analysis were conducted using HOMER (v4.9.1, <http://homer.ucsd.edu/homer/>). Sequencing signals were generated by transforming the mapping files into bigwig tracks and visualized in Integrated Genomic Viewers (University of California, San Diego, CA, USA).

### 2.15 | Animals and treatment

For xenograft mouse model, human peripheral blood mononuclear cell (Hu-PBMC) reconstruction mice were purchased from Shanghai Model Organisms Center (Shanghai, China). Briefly,  $5 \times 10^6$  MDA-MB-231 cells were suspended in normal saline and injected into the mammary fat pads of female NOD.Cg-*Prkdc<sup>scid</sup>Il2rg<sup>em1Smoc</sup>* mice aged 6 weeks. The mice lack mature T, B and NK cells and demonstrate low immune rejection against human cells and tissues [34]. Tumor sizes were monitored every 3 days. Tumor volume was calculated as  $\pi/6 \times \text{length} \times \text{width}^2$  ( $\text{mm}^3$ ). When the tumor volume reached 80-100  $\text{mm}^3$ ,  $5 \times 10^6$  Hu-PBMCs were intravenously engrafted. On average, the mice achieved efficient T cell reconstruction after 10 days and resulted in 15%-45% human CD45<sup>+</sup> cells in the mouse peripheral blood within 4 weeks, suitable to assess tumor immunotherapy [34]. The control group was treated with PBS and IgG, and the anti-PD-L1 treatment group was treated with PBS and atezolizumab (Ate) (HK-65567, F.Hoffmann-La Roche Ltd, Basel, Switzerland) 3 mg/kg twice a week for 2 weeks intraperitoneally [35]. For isograft mouse model,  $2 \times 10^6$  4T1 cells were suspended in normal saline and injected into the mammary fat pads of female BALB/c mice (Shanghai Model Organisms Center) aged 6 weeks. Tumor sizes were monitored and calculated as described above. All mice were maintained in specific pathogen-free cages and provided autoclaved food and water in accordance with the Accreditation of Laboratory Animal Care International Guidelines. Animals were humanely euthanized through  $\text{CO}_2$  overdose if the tumor burden was greater than 2,000  $\text{mm}^3$  or at the planned end point of the experiment. Animal experimental protocols were approved by the Animal Care Committee of Fudan University Shanghai Cancer Center (FUSCC, No. 2020FUSCCJS-237).

### 2.16 | Tumor tissue digestion and flow cytometry

Mouse mammary tumors were excised and divided into two parts for immunohistochemistry (IHC) and flow cytometry. For flow cytometry, tumor tissues were cut into small pieces and digested with 1 mg/mL collagenase type

IV (C5138, Sigma-Aldrich) and 0.6 ku/mL DNase (D5025, Sigma-Aldrich) for 2.5 h. Samples were then filtrated into single-cell suspensions and stained with CD45-FITC (1:20, 11-0451-82, eBioscience), CD8-PE (1:20, 12-0081-82, eBioscience), CD107-APC (1:20, MA5-28671, eBioscience) and CD69-PerCP-Cyanine5.5 (1:20, 45-0691-82, eBioscience). The results of flow cytometry were analyzed with FlowJo V10 (Becton Dickinson, Franklin Lakes, NJ, USA).

## 2.17 | Human tissue specimens

A set of tissue microarray (TMA) including 258 breast cancer tissue samples was obtained from the recruited breast cancer patients, diagnosed between August 2015 and December 2017, at their first radical surgery with no prior systemic neoadjuvant treatment. We included female patients who had been pathologically diagnosed only with breast cancer in their lifetime. Other inclusion criteria were age 18-90 years, of TNBC subtype (American Society of Clinical Oncology/College of American Pathologists guidelines [36, 37]), and with stage I-IIIa disease (the 8<sup>th</sup> edition of the Union for International Cancer Control TNM staging system [38]). Patients who did not receive standard adjuvant treatment or with history of autoimmune diseases were excluded. All patients were graded according to the Nottingham histologic scoring system [39]. The study design, endpoints and results of the CTR20191353 trial have been reported previously [40]. Resected specimens were macroscopically examined to determine the location and size of a tumor. Specimens for histology were fixed in 10% (v/v) formalin and processed for paraffin embedding. Overall survival (OS) was calculated from the date of surgery to the date of any-cause death or the last follow-up, whichever came first. Disease-free survival (DFS) was defined as the time interval from the date of surgery to the date of breast cancer recurrence or the last follow-up (June 2021), whichever came first. Progression-free survival (PFS) was defined as the time interval from the date of treatment with chemotherapy plus pucotenlimab to the date of breast cancer progression or the last follow-up, whichever came first. PFS-long and short patients were defined based on a 50% cutoff. Written informed consent was obtained from all patients, and all research protocols were approved by the medical ethics committee of FUSCC.

## 2.18 | Histopathology

The primary antibodies against ARID1A (1:1,000, sc-32761, Santa Cruz Biotechnology), CD8 (1:500, ab217344, Abcam), granzyme B (GB, 1:200, ab255598, Abcam), PD-L1 (1:60,

22C3, Dako, Hovedstaden, Denmark) or NPM1 (1:1,000) were incubated at 4°C overnight. TMA was scanned by a NanoZoomer HT 1.0 (Hamamatsu Photonics Co. Ltd, Hamamatsu, Shizuoka, Japan) and processed through the VIS DIA VisioMarph system (Visiopharm, Hoersholm, Denmark) according to the manufacturer's instructions. Five views were examined per core, and 100 cells were observed per view at 400 × magnification. TMA cores which contained <100 viable tumor cells were excluded. As immunohistochemical staining of ARID1A and NPM1 was primarily located in the nucleus of tumor cells, their protein levels were scored by the number of positive tumor cells divided by the total number of tumor cells. Level 0 to 3 of ARID1A expression were defined based on score quantiles, with 0 corresponding to the lowermost quantile and 3 corresponding to the uppermost quantile. ARID1A- and NPM1-high versus -low patients were classified based on a 50% cutoff. PD-L1 tumor proportion score (TPS) was defined as the number of positive tumor cells divided by the total number of viable tumor cells multiplied by 100, and combined positive score (CPS) was the number of positive tumor cells, lymphocytes and macrophages divided by the total number of viable tumor cells multiplied by 100 [41]. The CD8 and GB levels were determined as the number of positive cells divided by the total number of cells since both were mainly found in tumor-infiltrating lymphocytes (TILs). Tertiary lymphoid structures, necrosis and other immune infiltrates beyond the tumor border were excluded.

## 2.19 | Multispectral fluorescent IHC

Multiplexed immunofluorescent staining and multispectral image analysis were performed as previously described [42]. In brief, 4-mm-thick formalin-fixed paraffin-embedded slides were deparaffinized in a Leica auto-stainer (Leica Biosystems, Nussloch, Germany), and citrate buffer pH 6.0 (Shanghai Epizyme Biomedical Technology) was used for antigen retrieval. Slides were subsequently blocked with Antibody Diluent (BioGenex Laboratories, Fremont, CA, USA) and incubated with primary antibodies for 30 min at room temperature. Primary antibodies included ARID1A (1:300), CD8 (1:100, C8/1444B, Dako), GB (1:300), PD-L1 (1:100) and NPM1 (1:200). After washing with TBST, the slides were incubated with horseradish peroxidase-linked secondary antibodies (Life Technologies, Carlsbad, CA, USA). Afterwards, tyramide-conjugated fluorophores (Opal, PerkinElmer, Waltham, MA, USA) were added at a 1:50 dilution and incubated for 10 min at room temperature. This process was repeated for all 5 antibodies, and 4',6-diamidino-2'-phenylindole (Life Technologies)

was diluted at 1:500. Finally, slides were cover slipped with VECTASHIELD Hard Mount (Vector Laboratories, Burlingame, CA, USA). Scanning was performed with a Vectra automated multispectral microscope (PerkinElmer), and inForm software (PerkinElmer) was used for analysis.

## 2.20 | Gene set enrichment analysis (GSEA)

GSEA was performed using Java software GSEA v4.1.0 based on the Molecular Signature Database v7.2 (M9779, M9774, M1086; <https://www.gsea-msigdb.org/gsea/msigdb/index.jsp>) [43, 44]. Hits (gene set numbers) and misses (non-members) were scored with the “weighted” enrichment method, and the metric for ranking genes was the “Signal2Noise” method. All other parameters were set as default.

## 2.21 | Database and computational algorithms

A total of 251 epigenetic regulator proteins in *Homo sapiens* were retrieved from Gene Ontology Resource (GO:0040029, <http://geneontology.org>), and gene signatures for AIR were utilized to assess expression correlation [45–48]. All gene expression in TNBC was analyzed using The Cancer Genome Atlas (TCGA) data in cBioPortal (<https://www.cbioportal.org>), and *ARID1A*-high and -low patients were categorized based on a 50% cutoff [49]. Immune cell abundance in the breast tumor microenvironment was estimated using CIBERSORT [50], Thorsson [51] and TIMER2.0 computational algorithms [52]. Single-cell RNA-seq data for TNBC patients were obtained from the Gene Expression Omnibus (GEO) dataset GSE75688 (<https://www.ncbi.nlm.nih.gov/geo/>), and cells were profiled using Smart-seq2 [53]. The Seurat package (3.1.1, <https://cran.r-project.org/web/packages/Seurat/index.html>) was adopted for further analysis. Regulators for CD8<sup>+</sup> T cells were derived from Gene Ontology Resource (GO: 2001185, <http://geneontology.org>). Sequences of *PD-L1* and *NPM1* promoters and coding regions were obtained from the University of California Santa Cruz (UCSC) database (<https://genome.ucsc.edu>), and *PD-L1* and *NPM1* enhancers were predicted through EnhancerDB (<http://lcbj.swjtu.edu.cn/EnhancerDB/>). Transcription regulators for *PD-L1* were predicted through UCSC database (score range set as > 530), identifying 13 transcription regulators, and literature review was performed using PubMed (<https://pubmed.ncbi.nlm.nih.gov>) with the query “(“PD-L1” [Title/Abstract] OR “CD274”

[Title/Abstract]) AND (TNBC [Title/Abstract] OR “triple negative breast cancer” [Title/Abstract] OR “triple-negative breast cancer” [Title/Abstract]) AND (transcription [Title/Abstract] OR transcript [Title/Abstract] OR mRNA [Title/Abstract])” and returned 60 results. After detailed reading, we filtered out 47 irrelevant publications and summarized the relevant 13 publications (including 15 transcription regulators, 1 overlapping with UCSC prediction) as Supplementary Table S1. *ARID1A* and *BRG1* ChIP-seq data were obtained from the GEO datasets GSE72141 and GSE174360 (<https://www.ncbi.nlm.nih.gov/gds>). All sequencing data were viewed using UCSC genome browser.

## 2.22 | Statistical Analysis

All data were analyzed and graphed using GraphPad Prism 8 (Graphpad Software Inc, San Diego, CA, USA) or R 4.0.2 (<https://www.r-project.org>). Experimental data are presented as mean  $\pm$  standard deviation of three independent experiments. Two-group comparisons were conducted by two-sided Student’s *t*-test. The correlation analysis was conducted by Pearson correlation analysis. The Kaplan–Meier method was adopted for analyzing DFS, PFS and OS. All variables showing statistical significance in univariate regression were adopted for multiple regression via the Cox proportional hazards model.  $P < 0.05$  was considered statistically significant. Western blotting was repeated three times independently showing similar results.

## 3 | RESULTS

### 3.1 | Deficiency of the epigenetic modulator *ARID1A* contributed to AIR in TNBC

To explore epigenetic regulation for AIR in TNBC, we used RNA-seq data from TNBC patients in TCGA to analyze the association between the expression of 251 epigenetic genes and AIR signatures (Supplementary Table S2). The expression of *ARID1A* demonstrated the highest correlation with TNBC AIR among the epigenetic gene set, showing positive correlations with cytotoxic T cell function, lymphocyte infiltration, antigen presentation and IFN- $\gamma$  pathway score and a negative correlation with immune checkpoint score (Figure 1A, Supplementary Figure S1A). This suggested that low *ARID1A* in TNBC patients contributed to AIR, resulting in progressive tumor growth.

To verify this hypothesis, we evaluated the role of *ARID1A* in tumor progression using mouse models. Through knocking out and overexpressing *ARID1A* in

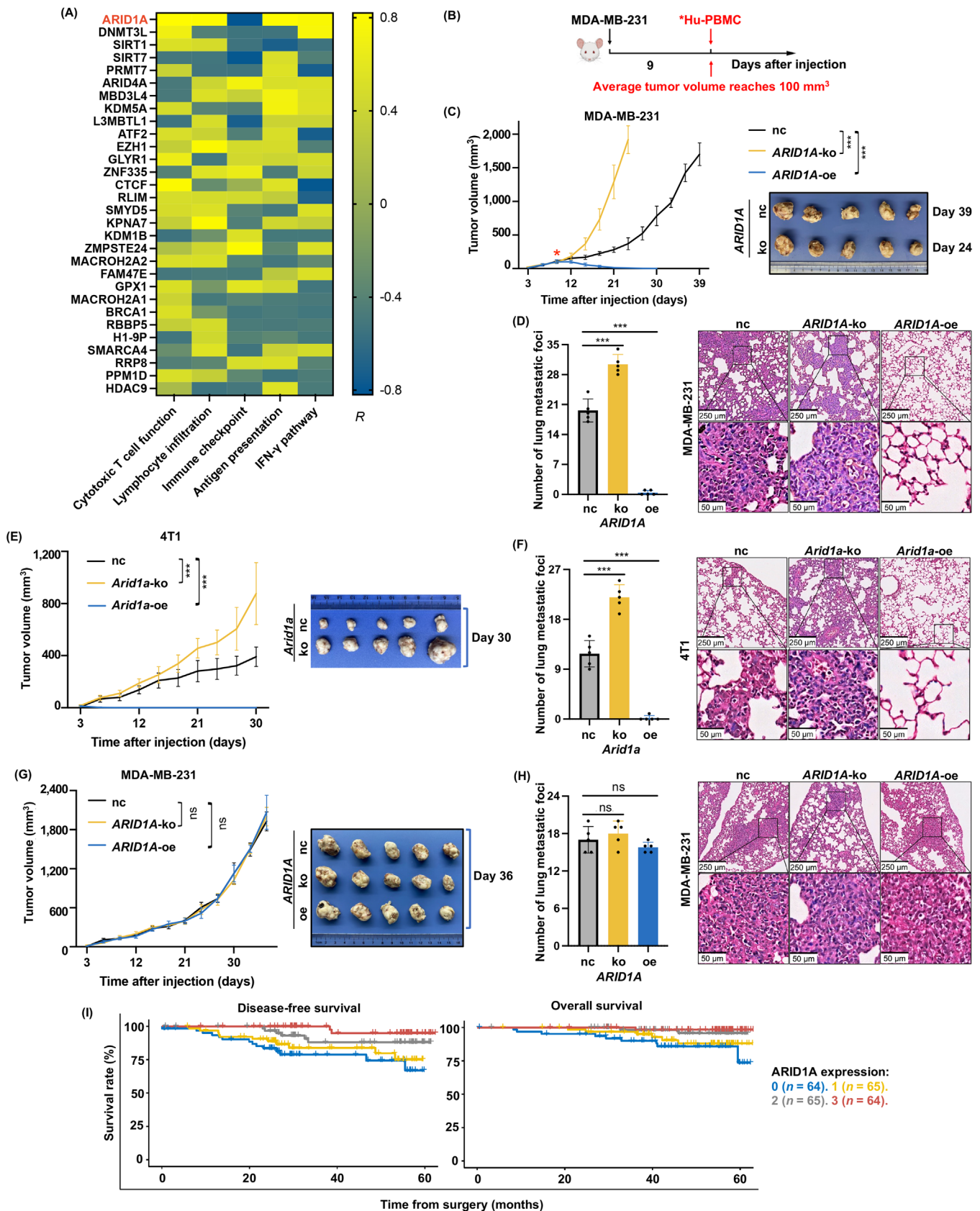


**FIGURE 1** Deficiency of the epigenetic modulator ARID1A in TNBC contributed to AIR. (A) Heat map showing top 30 epigenetic modulators of highest expression correlation with AIR in TNBC. Yellow and blue depict positive and negative correlation, respectively. (B) Schematic diagram of Hu-PBMC reconstruction mice ( $n = 5$  for each group). Black arrow: injection of MDA-MB-231 cells into the mammary fat pads. \* Hu-PBMC engraftment when average tumor volume reaches 100 mm<sup>3</sup> (day 9). (C) Average tumor volume depicted over time in

MDA-MB-231 cells (Supplementary Figure S1B), we found that *ARID1A* knockout significantly increased both tumor growth and the number of lung metastatic foci in Hu-PBMC reconstruction mice (Figure 1B-D). The tumors grew to the approximate size of 2,000 mm<sup>3</sup> at day 24 and day 39 after TNBC cell injection in knockout and negative control groups, respectively (Figure 1C). Interestingly, *ARID1A*-oe tumors gradually diminished after Hu-PBMC engraftment, and few metastatic foci were found in the lungs. For analysis in immunocompetent settings through preclinical mouse models, we further constructed *Arid1a*-ko and -oe 4T1 cells and performed transplantation using BALB/c mice (Supplementary Figure S1C). Both tumor growth and lung metastasis in recipient mice were found dramatically increased in *Arid1a*-ko group, whereas *Arid1a*-oe 4T1 cells failed to form tumors and developed few lung metastatic foci (Figure 1E-F). Notably, in nude mice without Hu-PBMC reconstruction, no difference in tumor growth or lung metastasis was observed among *ARID1A*-ko, -oe and negative control groups engrafted with MDA-MB-231 cells (Figure 1G-H). We also compared tumor growth in Hu-PBMC and non-Hu-PBMC conditions (Supplementary Figure S1D). For negative control MDA-MB-231 cells, Hu-PBMC reconstruction inhibited tumor growth relative to nude mice. For *ARID1A*-ko MDA-MB-231 cells, tumors in Hu-PBMC reconstruction mice demonstrated significantly faster growth as well as more frequent lung metastasis than in nude mice. For further validation in vitro, we found that *ARID1A* status did not affect colony formation, cell proliferation or apoptosis of two TNBC cell lines, MDA-MB-231 and MDA-MB-468, in the absence of lymphocytes (Supplementary Figure S1E-H). These results indicated immunity as the determinant for low *ARID1A* expression-triggered TNBC progression.

To validate the role of *ARID1A* in AIR using our own cohort, we included a 258-TNBC patient cohort from FUSCC. Through analyzing associations between *ARID1A* expression and tumor malignancy and prognosis of TNBC, we found that patients with lower *ARID1A* demonstrated larger tumor size, more frequent lymph node invasion,

higher KI67 and more advanced tumor grade than patients with higher *ARID1A* (Table 1, Supplementary Figure S1I). In survival analyses, low *ARID1A* in TNBC was identified as an independent poor prognostic factor for both DFS and OS (Figure 1I, Supplementary Tables S3-S4).

We also assessed the relationship between the protein level and mutations and copy number alterations of *ARID1A* in TNBC using the data from TCGA database. We found that no patient possessed high-level copy number amplification (CN2) or homozygous deletion (CN-2). Meanwhile, 20.2% (24/119), 36.1% (43/119) and 43.7% (52/119) patients showed low levels of copy number gain (CN1), hemizygous deletion (CN-1) and no change (CN0), respectively. In addition, we found that the protein levels of *ARID1A* in both CN0 ( $P = 0.007$ ) and CN1 patients ( $P = 0.006$ ) were significantly higher than that in CN-1 patients (Supplementary Figure S1J). Based on a 50% cutoff for protein expression, 64.3% CN-1, 45.8% CN1 and 37.2% CN0 patients were in *ARID1A*-low group (CN-1 vs. CN1,  $P < 0.001$ ; CN-1 vs. CN0,  $P < 0.001$ ; CN1 vs. CN0,  $P = 0.075$ ). In addition, among the 119 TNBC patients, only 2 (1.68%) harbored *ARID1A* mutations. One was Y2031\*, categorized as nonsense, and the other was *ARID1A* X1136\_splice. It was noteworthy that the latter patient also demonstrated *ARID1A* CN-1, and both patients were categorized as *ARID1A*-low based on the 50% cutoff for protein expression. Therefore, we consider that categorizing TNBC patients by *ARID1A* protein level has taken into account the impact of *ARID1A* mutation and copy number alteration.

Taken together, low expression of the epigenetic modulator *ARID1A* contributed to AIR in TNBC, leading to tumor progression.

### 3.2 | *ARID1A* deficiency inhibited CD8<sup>+</sup> T cells to enhance AIR in TNBC

To further explore the role of *ARID1A* in AIR regulation, we focused on the relationship between *ARID1A* and

Hu-PBMC reconstruction mice ( $n = 5$  for each group, left) and tumor image at the end of experiment (right, negative control: day 39; knockout: day 24). (D) Quantification of lung metastatic foci (left) and representative HE staining (right) as in (C). (E) Average tumor volume of 4T1 cells injected into BALB/c mice depicted over time ( $n = 5$  for each group, left) and tumor image at the end of experiment (right, day 30 for all experimental groups). (F) Quantification of lung metastatic foci (left) and representative HE staining (right) as in (E). (G) Average tumor volume of MDA-MB-231 cells injected into nude mice depicted over time ( $n = 5$  for each group, left) and tumor image at the end of experiment (right, day 36 for all experiment groups). (H) Quantification of lung metastatic foci (left) and representative HE staining (right) as in (G). (I) Kaplan–Meier analysis for DFS (left) and OS (right) based on *ARID1A* expression in the FUSCC TNBC cohort TMA. 0 to 3 represent the lowest to highest *ARID1A* expression groups. \*\*\* $P < 0.001$ , ns not significantly different.

Abbreviations: *ARID1A*, AT-rich interaction domain 1A; AIR, adaptive immune resistance; TNBC, triple-negative breast cancer; Hu-PBMC, human peripheral blood mononuclear cell; ko, knockout; oe, overexpression; nc, negative control; HE, hematoxylin-eosin; DFS, disease-free survival; OS, overall survival; FUSCC, Fudan University Shanghai Cancer Center; TMA, tissue microarray.

**TABLE 1** Characteristics of 258 patients with TNBC in the FUSCC cohort.

Characteristic	Total population [cases (%)]	ARID1A-high [cases (%)]	ARID1A-low [cases (%)]	P <sup>a</sup>
Total	258 (100)	128 (49.4)	130 (50.2)	
Age at diagnosis				
18-34 years	17 (6.6)	4 (3.1)	13 (10.0)	0.042
≥ 35 years	241 (93.4)	124 (96.9)	117 (90.0)	
T stage				
T1	106 (41.1)	62 (48.4)	44 (33.8)	0.023
T2-3	152 (58.9)	66 (51.6)	86 (66.2)	
Lymph node metastasis				
Negative	132 (51.2)	75 (58.6)	57 (43.8)	0.019
Positive	126 (48.8)	53 (41.4)	73 (56.2)	
KI67 expression <sup>b</sup>				
Low	57 (22.1)	36 (28.1)	21 (16.2)	0.024
High	201 (77.9)	92 (71.9)	109 (83.8)	
Histological grade				
I	17 (6.6)	13 (10.2)	4 (3.1)	0.025
II	118 (45.7)	62 (48.4)	56 (43.1)	
III	123 (47.7)	53 (41.4)	70 (53.8)	
Vascular invasion				
Negative	158 (61.2)	81 (63.3)	77 (59.2)	0.446
Positive	100 (38.8)	47 (36.7)	53 (40.8)	

<sup>a</sup>Differences between ARID1A-high and ARID1A-low were compared using the Pearson's Chi-square test.

<sup>b</sup>KI67 low ≤ 20%, high > 20%

immune cells in the tumor immune microenvironment (TIME) through CIBERSORT computational algorithm. We found that *ARID1A* expression in TNBC tissue was positively associated with infiltration of CD8<sup>+</sup> T cells, T follicular helper cells and M1 macrophages, and negatively correlated with infiltration of regulatory T cells and M2 macrophages. Compared with other immune cell types, CD8<sup>+</sup> T cells were found to be the most significantly correlated with *ARID1A* expression in TCGA (Figure 2A). This was further supported by single-cell RNA-seq in 5 TNBC patients, as well as Thorsson and TIMER computational algorithms (Figure 2B-C, Supplementary Figure S2A-B). GSEA also showed CD8<sup>+</sup> T cell inactivation to be significantly associated with low *ARID1A* expression (Figure 2D). Therefore, we hypothesized that CD8<sup>+</sup> T cells might be the key factor for low *ARID1A* expression-induced AIR in TNBC.

We further explored the relationship between *ARID1A* expression and CD8<sup>+</sup> T cells in tumor samples from the FUSCC TNBC cohort and from the above-described mouse models through analyzing CD8 and GB expression. In accordance with transcriptome data, the protein levels of CD8 and GB were much lower in *ARID1A*-low tumors, indicating inhibited CD8<sup>+</sup> T cell infiltration and activation (Figure 2E-F, Supplementary Figure S2C). To verify the

function of *ARID1A* in vitro, two types of T cells, Jurkat and primary T cells, were cocultured with TNBC cells differentially expressing *ARID1A*. ELISA showed that the secretion of IL-2 by Jurkat cells was dramatically decreased when cocultured with *ARID1A*-ko TNBC cells compared to those cocultured with negative control TNBC cells. Similarly, *ARID1A* silencing in TNBC cells significantly decreased the percentage of IFN- $\gamma$ -producing primary T cells. Opposite effects of *ARID1A* overexpression on T cells were found (Figure 2G, Supplementary Figure S2D). Taken together, TNBC cells with *ARID1A* low expression inhibited CD8<sup>+</sup> T cells in TIME.

### 3.3 | PD-L1 mediated *ARID1A* low expression-induced CD8<sup>+</sup> T cell inactivation

To probe the mechanisms underlying low *ARID1A* expression-induced CD8<sup>+</sup> T cell malfunction and AIR, we focused on 21 CD8<sup>+</sup> T cell regulators derived from the Gene Ontology Resource (GO:2001185), including 12 positive and 9 negative regulators. Expression of these genes was examined through RNA-seq in TCGA TNBC patients (*ARID1A*-low versus -high) and MDA-MB-231

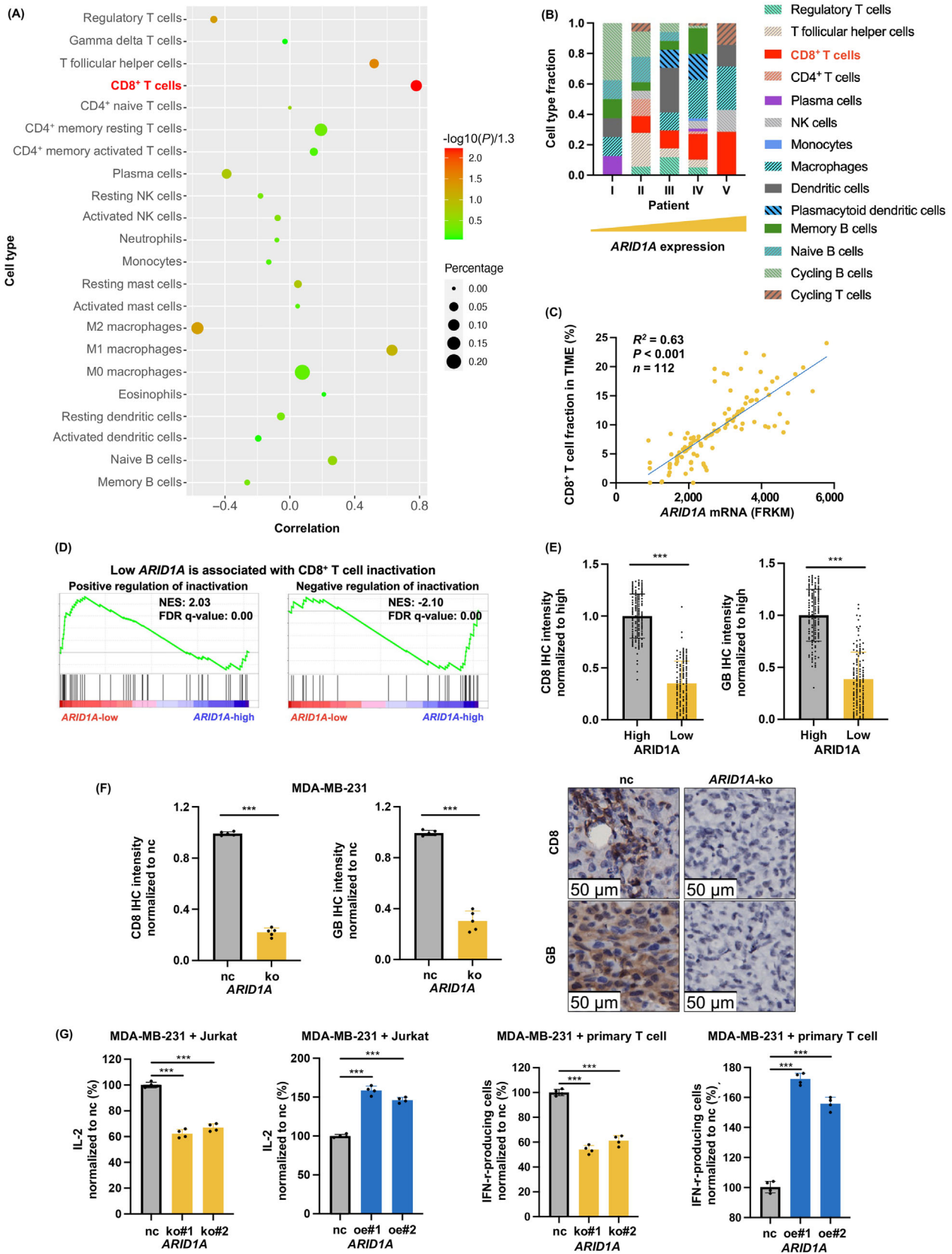


**FIGURE 2** TNBC *ARID1A* deficiency inhibited CD8<sup>+</sup> T cells to enhance AIR. (A) CIBERSORT analysis showing correlation of *ARID1A* with immune cell abundance in TCGA. Red and green depict lower and higher  $P$  values, respectively, and circle size represent the percentage of immune cells. (B) Bar plot showing the fraction of immune cells in 5 TNBC patients using single cell RNA-seq. The patients were numbered according to *ARID1A* expression in TNBC. Yellow triangle (down) represented lower to higher *ARID1A* expression in patient

cells (*ARID1A*-ko versus negative control) by calculating the fold change (Figure 3A, Supplementary Figure S3A). Except for SH3 domain containing ring finger 1 (*SH3RF1*) and mitogen-activated protein kinase 8 interacting protein 1 (*MAPK8IP1*), 11 positive and 8 negative regulators were significantly decreased and increased in *ARID1A*-low patients and *ARID1A*-ko cells, respectively. After mapping RNA-seq q values of the 19 candidate genes in TCGA patients to the x-axis, and those of MDA-MB-231 cells to the y-axis, *PD-L1* was identified to be the candidate gene furthest from the origin (Figure 3B).

Next, qPCR, Western blotting and flow cytometry all confirmed notably high PD-L1 expression on the TNBC cell membrane in the *ARID1A*-ko group, while the opposite variations were observed in *ARID1A*-oe TNBC cells (Figure 3C-D, Supplementary Figure S3B-D). In the FUSCC TNBC cohort, *ARID1A*-low patients showed higher PD-L1 levels both in TPS and CPS compared with *ARID1A*-high counterparts (Figure 3E). In addition, we found that the protein level of PD-L1 was higher in *ARID1A*-ko tumor samples from MDA-MB-231 Hu-PBMC mice and 4T1 BALB/c mice than that of negative control groups (Figure 3F, Supplementary Figure S3E).

To further assess whether PD-L1 mediated low *ARID1A* expression-induced CD8<sup>+</sup> T inactivation, we knocked down *PD-L1* in *ARID1A*-ko TNBC cells (Supplementary Figure S3F) and performed coculture assays with T lymphocytes. The activity of both Jurkat and primary T cells, though dampened by *ARID1A*-ko TNBC cells relative to negative control TNBC cells, were rescued by *ARID1A*-ko/*shPD-L1* TNBC cells (Supplementary Figure S3G). Further, we overexpressed *PD-L1* in *ARID1A*-oe MDA-MB-231 (Supplementary Figure S3H) and evaluated the role of PD-L1 in rescuing tumor growth in vivo under *ARID1A*-oe condition (Figure 3G). Similar to previous observations, *ARID1A*-ko tumors demonstrated faster growth as well as a higher frequency of lung metastasis compared with negative control. However, in *ARID1A*-ko tumors coharboring *shPD-L1*, both tumor growth and lung metastasis were significantly decreased. While

*ARID1A*-oe tumors failed to maintain growth after Hu-PBMC engraftment and demonstrated few lung metastatic foci, *ARID1A*-oe/*PD-L1*-oe tumors demonstrated faster growth as well as higher frequency of lung metastasis (Figure 3G, Supplementary Figure S4A). We also found that CD8 and GB were decreased in *ARID1A*-ko tumors but were rescued by *shPD-L1* (Figure 3H, Supplementary Figure S4B).

The above in vitro and in vivo results indicated that PD-L1, induced by low *ARID1A* expression, inhibited CD8<sup>+</sup> T cells and led to AIR.

### 3.4 | Low *ARID1A* expression activated *PD-L1* transcription, while *ARID1A* did not bind to *PD-L1* promoter or enhancer

To elucidate how *ARID1A* inhibited PD-L1 expression, ChIP-seq was performed with antibodies against H3K4me3 (indicative of active promoters). In the promoter region of *PD-L1*, signals were markedly increased in *ARID1A*-ko cells (Figure 4A), which was further confirmed by ChIP-qPCR (Figure 4B). Dual luciferase reporter assay demonstrated corresponding variations in *PD-L1* promoter activity (Figure 4C-D), with an irrelevant promoter (activin A receptor type 1, *FOP*) as the negative control to confirm specificity in *ARID1A*'s regulatory activity (Supplementary Figure S5A). These results led to the conclusion that *ARID1A* deficiency activated *PD-L1* transcription.

We next examined whether *ARID1A* directly binds to the *PD-L1* promoter to regulate its expression and analyzed ChIP-seq data for *ARID1A* and BRG1, another key component of SWI/SNF, in MDA-MB-231 cells. However, we failed to identify *ARID1A*- or BRG1-binding sites in the *PD-L1* promoter (Figure 4E), while *FBXO38*, a positive control, demonstrated obvious peaks in its promoter region (Supplementary Figure S5B). This negative result was also confirmed by ChIP-qPCR and ChIP-PCR (Supplementary Figure S5C-D), while binding sites in *FBXO38* promoter

Number I to V. (C) Scatter plot depicting the relationship between *ARID1A* mRNA level as measured by RNA-seq and CD8<sup>+</sup> T cell percentage in TIME in TCGA. (D) GSEA plot showing low *ARID1A* expression-induced genes enriched for CD8<sup>+</sup> T cell inactivation in TNBC patients. (E) Comparison of CD8<sup>+</sup> T cell markers CD8 and GB by *ARID1A* expression in the FUSCC TNBC cohort TMA. (F) Quantification (left) and representative images (right) of CD8<sup>+</sup> T cell markers CD8 and GB IHC in Hu-PBMC tumor tissue. (G) Jurkat cells were cocultured with MDA-MB-231 cells and IL-2 secretion was detected by ELISA. Primary T cells were cocultured with MDA-MB-231 cells and IFN- $\gamma$ -producing T cells were detected by flow cytometry. \*\*\**P* < 0.001.

Abbreviations: *ARID1A*, AT-rich interaction domain 1A; AIR, adaptive immune resistance; TCGA, The Cancer Genome Atlas; TNBC, triple-negative breast cancer; RNA-seq, RNA sequencing; TIME, tumor immune microenvironment; GSEA, gene set enrichment analysis; GB, granzyme B; FUSCC, Fudan University Shanghai Cancer Center; TMA, tissue microarray; IHC, immunohistochemistry staining; Hu-PBMC, human peripheral blood mononuclear cell; ko, knockout; nc, negative control; ELISA, enzyme linked immunosorbent assay; FPKM, fragments per kilobase million; NES, normalized enrichment score; FDR, false discovery rate.

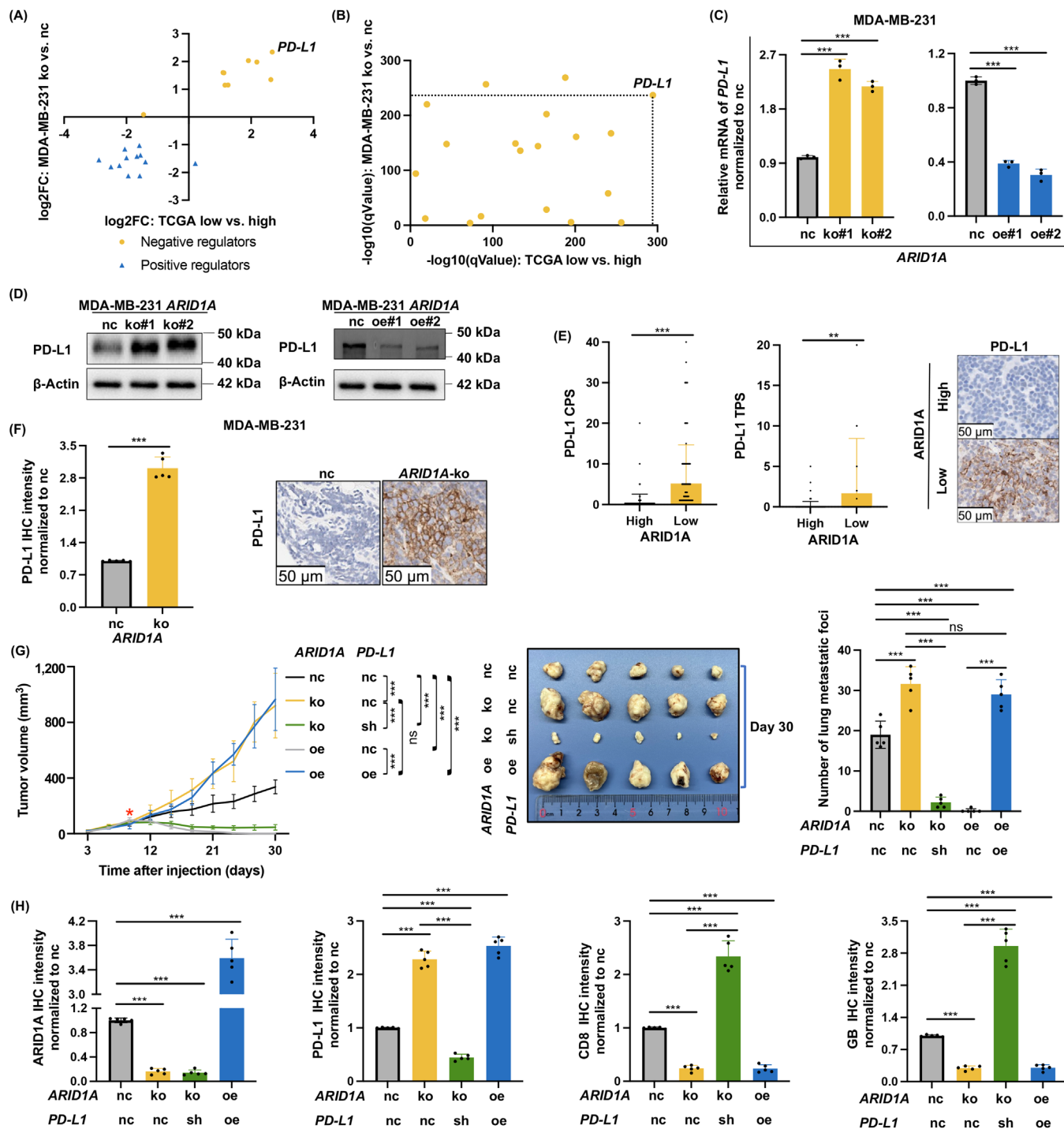


**FIGURE 3** PD-L1 mediated *ARID1A* low expression-induced CD8<sup>+</sup> T cell inactivation. (A) Scatter plot showing expression variation of CD8<sup>+</sup> T cell-modulating genes in *ARID1A*-low versus high TNBC patients in TCGA (x-axis), as well as in *ARID1A*-ko versus negative control MDA-MB-231 cells (y-axis). (B) A log<sub>10</sub>-qValue plot of screening results in (A). The RNA-seq q value of the 19 candidate genes in *ARID1A*-low versus high TCGA TNBC patients was mapped to the x-axis and that of *ARID1A*-ko versus negative control MDA-MB-231 cells was mapped to the y-axis. (C) qPCR for *PD-L1* following *ARID1A*-ko and -oe in MDA-MB-231 cells. (D) Western blotting for PD-L1 following *ARID1A* knockout and overexpression in MDA-MB-231 cells. (E) Quantification (left) and representative images (right) of PD-L1 CPS and TPS by *ARID1A* expression in the FUSCC TNBC cohort TMA. (F) Quantification (left) and representative images (right) of PD-L1 IHC in Hu-PBMC tumor tissue. (G) Average tumor volume of MDA-MB-231 cells with different *ARID1A* and *PD-L1* expression status injected into Hu-PBMC reconstruction mice depicted over time ( $n = 5$  for each group, up) and tumor image at the end of experiment (down left, day 30 for all experimental groups), with quantification of lung metastatic foci (down right). (H) Quantification of *ARID1A*, *PD-L1*, *CD8* and *GB* IHC in tumor tissue from (H). \*\* $P < 0.01$ , \*\*\* $P < 0.001$ , ns not significantly different.

could be confirmed (Supplementary Figure S5E). We also checked *PD-L1* enhancers (Supplementary Table S5) for ARID1A and BRG1 binding and found only 1 was bound by BRG1, while no ARID1A-binding peak was observed (Supplementary Figure S6A). In addition, ChIP-qPCR and ChIP-PCR for ARID1A and BRG1 failed to validate direct binding for this enhancer in TNBC cell lines (Supplementary Figure S6B). We further performed ATAC-seq to assess the chromatin accessibility of *PD-L1* in MDA-MB-231 cells and found no significant alteration induced by *ARID1A*-ko (Figure 4F). To explore the potential regulatory mechanism underlying low ARID1A expression-induced *PD-L1* transcription activation, we also performed ChIP-seq for enhancer-specific histone markers H3K4me1 and H3K27ac in *ARID1A*-ko and negative control MDA-MB-231 cells, and conducted pathway analyses in H3K4me3, H3K4me1 and H3K27ac ChIP-seq as well as ATAC-seq. We found that the differential H3K4me3 signal distribution between *ARID1A*-ko and negative control cells were enriched in AIR-related pathways, including the “T cell receptor signaling pathway” and “antigen processing and presentation”, both ranked top 10 among a series of pathways. As for ATAC-seq, top 10 enriched pathways also included the “T cell receptor signaling pathway” (Figure 4G). In H3K4me1 and H3K27ac ChIP-seq, however, AIR was not among the top-ranked enriched pathways (Supplementary Figure S6C). This further suggested that ARID1A may regulate AIR in TNBC predominantly through promoter-binding and chromatin remodeling.

Taken together, the stimulatory effect of low ARID1A expression on *PD-L1* transcription may be achieved indirectly and possibility associated with promoter-binding and chromatin remodeling.

### 3.5 | Low ARID1A expression increased NPM1 to activate *PD-L1* transcription in TNBC

We thus focused on the transcriptional regulators of *PD-L1*. Through literature and UCSC Genome Browser, we identified 27 transcription regulators (Supplementary Table S1). Except for interferon regulatory factor 7 (IRF7), all were reported to elevate *PD-L1* expression. Among the positive regulators, only 4 were increased in *ARID1A*-ko MDA-MB-231 cells compared to negative control group,

while the expression of *IRF7* decreased in *ARID1A*-ko cells. Among these 5 candidates, only *NPM1* possessed both ARID1A- and BRG1-binding sites at the promoter region according to ARID1A and BRG1 ChIP-seq (Figure 5A, Supplementary Figure S7A). Furthermore, TCGA TNBC data showed a negative correlation between *NPM1* and *ARID1A* mRNA (Supplementary Figure S7B), and GSEA demonstrated enrichment of the *NPM1* neighborhood in *ARID1A*-ko MDA-MB-231 cells relative to negative control (Supplementary Figure S7C). Therefore, we hypothesized that ARID1A directly bound to the *NPM1* promoter and inhibited its transcription, further resulting in a *PD-L1* decrease.

Indeed, we found a remarkable *NPM1* increase in *ARID1A*-ko cells through both qPCR and Western blotting, while a *NPM1* decrease was observed in *ARID1A*-oe cells (Figure 5B, Supplementary Figure S7D-E). Higher *NPM1* expression was also found in ARID1A-low TNBC patients compared to ARID1A-high counterparts (Figure 5C), as well as in *ARID1A*-ko tumors relative to negative control from MDA-MB-231 Hu-PBMC mice and 4T1 BALB/c mice (Supplementary Figure S7F-G). To further assess whether ARID1A downregulation activated *NPM1* transcription, we analyzed H3K4me3 ChIP-seq data and found enriched signals in the *NPM1* promoter region in *ARID1A*-ko cells (Figure 5D). H3K4me3 ChIP-qPCR (Supplementary Figure S7H), as well as luciferase reporter assays targeting the *NPM1* promoter (Figure 5E, Supplementary Figure S7I), also showed enhanced transcriptional activity. Using antibodies against ARID1A and BRG1, we confirmed direct binding of ARID1A to the *NPM1* promoter (Supplementary Figure S8A). ATAC-seq profiles showed that chromatin accessibility at *NPM1*, particularly in its promoter, was increased in *ARID1A*-ko MDA-MB-231 cells compared with negative control (Figure 5F). We also checked whether ARID1A or BRG1 bound to *NPM1* enhancers but found no binding peaks through ChIP-seq (Supplementary Table S6). In addition, the binding of *NPM1* to the *PD-L1* promoter was significantly elevated in *ARID1A*-ko cells relative to negative control (Supplementary Figure S8B). Finally, the increase in *PD-L1* expression in *ARID1A*-ko cells was reversed by sh*NPM1* (Figure 5G-H, Supplementary Figure S8C), and impaired T cell activity induced by *ARID1A*-ko TNBC cells compared to negative control was restored through sh*NPM1* in TNBC cells (Figure 5I). Taken together, ARID1A directly bound to the *NPM1* promoter

Abbreviations: PD-L1, programmed cell death 1 ligand 1; ARID1A, AT-rich interaction domain 1A; TNBC, triple-negative breast cancer; TCGA, The Cancer Genome Atlas; ko, knockout; oe, overexpression; sh, short hairpin RNA-mediated knockdown; nc, negative control; qPCR, quantitative real-time PCR; CPS, combined positive score; TPS, tumor proportion score; FUSCC, Fudan University Shanghai Cancer Center; TMA, tissue microarray; IHC, immunohistochemistry staining; Hu-PBMC, human peripheral blood mononuclear cell; GB, granzyme B; FC, fold change; vs., versus.

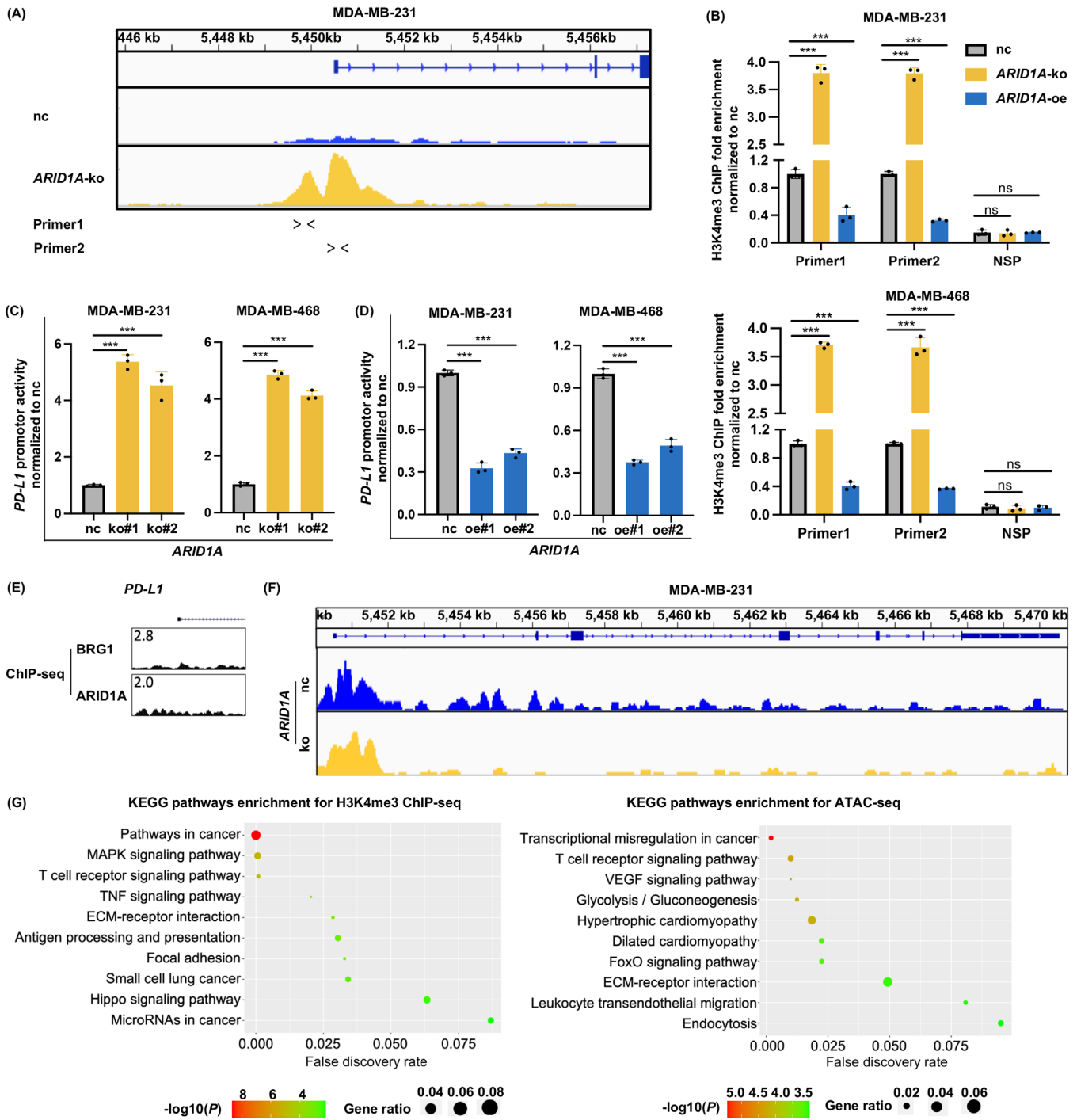


**FIGURE 4** Low ARID1A activated *PD-L1* transcription, while ARID1A did not bind to *PD-L1* promoter or enhancer. (A) Signal track of H3K4me3 ChIP-seq for *PD-L1* in ARID1A-ko and negative control MDA-MB-231 cells. (B) H3K4me3 ChIP-qPCR for *PD-L1*. Primer1 and 2 are located according to arrows in (A). NSP, nonspecific primer at the open reading frame-free region. (C) *PD-L1* promoter activity measured by dual-luciferase assay in ARID1A-ko versus negative control human TNBC cells. (D) *PD-L1* promoter activity measured by dual-luciferase assay in ARID1A-oe versus negative control human TNBC cells. (E) ARID1A (down) and BRG1 (up) ChIP-seq for *PD-L1* promoter. (F) ATAC-seq profiles for *PD-L1* in ARID1A-ko and negative control MDA-MB-231 cells showing similar chromatin accessibility. (G) Pathway enrichment plot for H3K4me3 ChIP-seq (left) and ATAC-seq (right) in ARID1A-ko versus negative control MDA-MB-231 cells. \*\*\* $P < 0.001$ , ns not significantly different.

Abbreviations: ARID1A, AT-rich interaction domain 1A; PD-L1, programmed cell death 1 ligand 1; ko, knockout; oe, overexpression; nc, negative control; TNBC, triple-negative breast cancer; ChIP, chromatin immunoprecipitation; qPCR, quantitative real-time PCR; BRG1, SWI/SNF related, matrix associated, actin dependent regulator of chromatin, subfamily a, member 4; ATAC, assay for transposase accessible chromatin; KEGG, Kyoto Encyclopedia of Genes and Genomes.

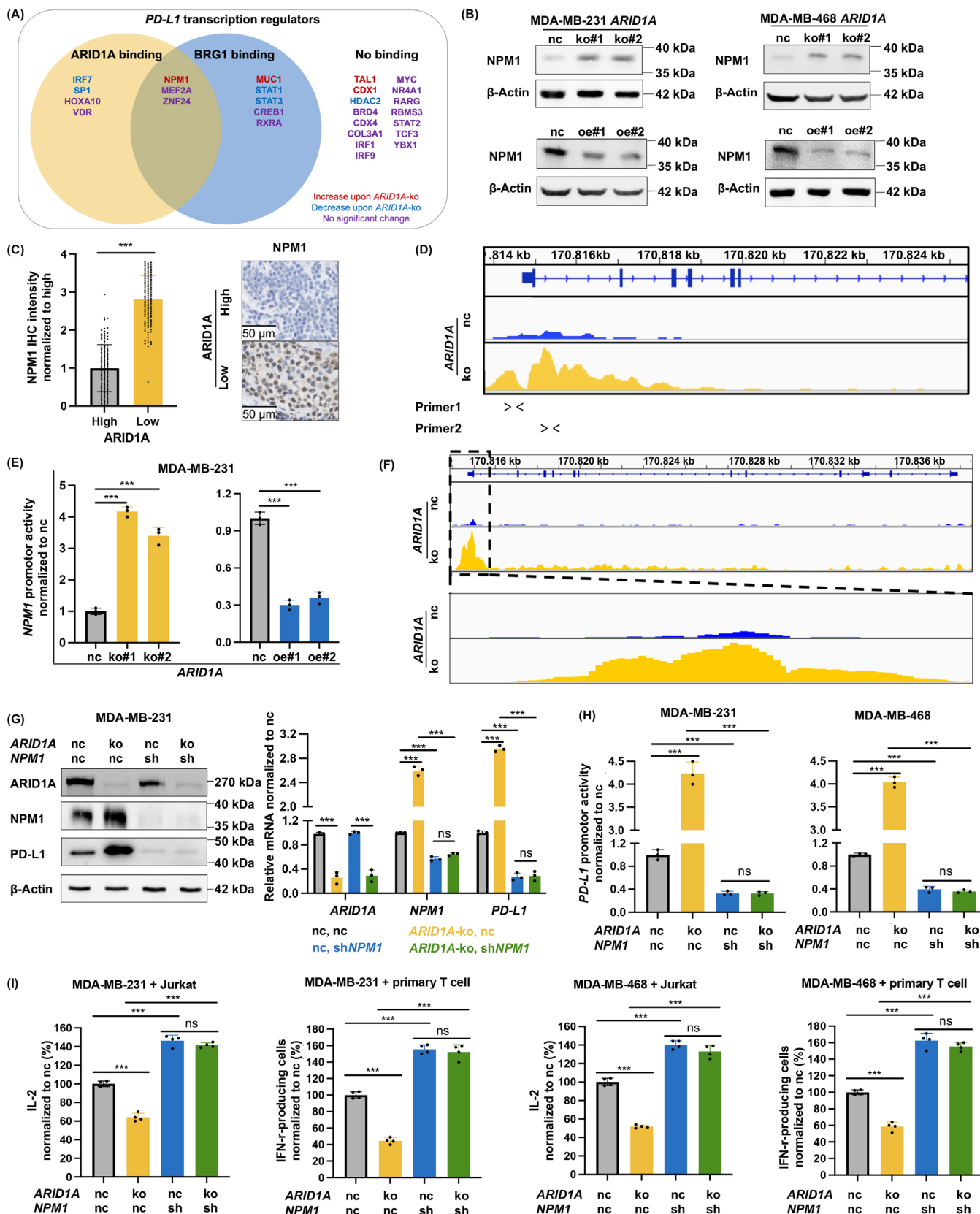


**FIGURE 5** ARID1A low expression increased NPM1 to activate PD-L1 transcription in TNBC. (A) Transcription regulators for PD-L1. Locations in Venn diagram indicate promoter binding by ARID1A and BRG1. Colors denote expression variation induced by ARID1A-ko in MDA-MB-231 cells. (B) Western blotting for NPM1 following ARID1A-ko (up) and -oe (down) in human TNBC cells. (C) Quantification (left) and representative images (right) of NPM1 IHC in the FUSCC TNBC cohort TMA. (D) Signal track of H3K4me3 ChIP-seq for NPM1 in

and its deficiency activated *NPM1* transcription, promoting PD-L1 expression and inhibiting CD8<sup>+</sup> T cells.

### 3.6 | ARID1A low expression-induced AIR and PD-L1 elevation in TNBC could be targeted by ICI

To explore the clinical significance of ARID1A deficiency-induced PD-L1 elevation and AIR, we treated the Hu-PBMC reconstruction mice with Ate, a PD-L1 antibody (Figure 6A). Again, *ARID1A*-ko led to faster tumor growth and more frequent pulmonary metastasis relative to negative control. However, after being treated with Ate twice a week for two doses, dramatic reductions in both tumor volume and pulmonary metastasis were observed for the *ARID1A*-ko group, while negative control group showed no sign of remission (Figure 6B-C, Supplementary Figure S9A). This suggested that ARID1A-deficient tumors, though demonstrating a more aggressive nature, responded much better to ICI treatment compared with ARID1A-proficient tumors.

To confirm the status of the PD-1/PD-L1 axis and CD8<sup>+</sup> T cells in response to Ate, TILs in the Hu-PBMC model were analyzed by flow cytometry (Supplementary Figure S9B). After being gated by the leukocyte common antigen CD45, the percentage of CD8<sup>+</sup> T cells was shown to be lower in *ARID1A*-ko tumors compared to negative control. Since activated CD8<sup>+</sup> T cells coexpress CD69 and CD107, we further analyzed CD8<sup>+</sup>CD69<sup>+</sup> and CD8<sup>+</sup>CD107<sup>+</sup> cell populations and found, in accordance with CD8<sup>+</sup> T cells, that both were lower in *ARID1A*-ko tumors relative to negative control (Supplementary Figure S9C). In addition, IHC confirmed decreased CD8<sup>+</sup> T cell markers for anti-tumor immune response along with elevated PD-L1 and *NPM1* in *ARID1A*-ko tumors relative to negative control (Supplementary Figure S9D). Ate significantly increased CD45<sup>+</sup> CD8<sup>+</sup> T cell population in ARID1A-deficient tumors but failed to achieve this in the control group. This was also the case with CD107<sup>+</sup> and CD69<sup>+</sup> T cells. IHC also confirmed a higher ratio and enhanced activity of T cells in

*ARID1A*-ko tumors compared to negative control tumors after treatment with Ate (Supplementary Figure S9C-D).

To further explore whether AIR and PD-L1 elevation induced by ARID1A low expression could pose a therapeutic vulnerability, tumor tissues from patients with metastatic TNBC enrolled in the CTR20191353 clinical trial were analyzed. In total, 31 patients received pucotenlimab (a humanized anti-PD-1 antagonist IgG4 monoclonal antibody) plus gemcitabine and cisplatin treatment. Patients with low ARID1A expression in TNBC demonstrated significantly longer PFS. Notably, the longest PFS of 615 days was found in ARID1A-low/PD-L1-high group (Figure 6D). Next, multispectral fluorescent IHC showed that patients with longer PFS demonstrated lower ARID1A expression and CD8<sup>+</sup> T cell infiltration compared to those with shorter PFS, whereas the expression of both PD-L1 and *NPM1* were significantly higher (Figure 6E).

Taken together, the above results indicated that AIR and PD-L1 expression in TNBC contributed by low level of ARID1A could be potentially reversed by ICIs, such as Ate and pucotenlimab (Figure 7).

## 4 | DISCUSSION

In the present study, ARID1A was found among a series of epigenetic modulators to be highly related to AIR in TNBC. We observed that low ARID1A expression inhibited CD8<sup>+</sup> T cell infiltration and activation and led to early progression in both clinical samples and xenograft models. PD-L1 upregulation was found to promote AIR in TNBC with low ARID1A expression. While no direct interaction was observed between ARID1A and *PD-L1* promoter, ARID1A was demonstrated to directly bind to the promoter of *NPM1*, further activating *PD-L1* transcription. This ARID1A/*NPM1*/PD-L1 axis was consolidated in both early and metastatic TNBC samples. Finally, we assessed the targetability of AIR in TNBC with low level of ARID1A by ICI treatment including Ate and pucotenlimab.

Notably, ARID1A-low TNBC demonstrated a better response to ICI treatment relative to ARID1A-high

*ARID1A*-ko and negative control MDA-MB-231 cells. (E) *NPM1* promoter activity measured by dual-luciferase assay in *ARID1A*-ko (left) and -oe (right) MDA-MB-231 cells. (F) ATAC-seq profiles for *NPM1* in *ARID1A*-ko and negative control MDA-MB-231 cells showing altered chromatin accessibility. (G) Western blotting (left) and qPCR (right) for PD-L1 in *ARID1A*-ko and sh*NPM1* MDA-MB-231 cells. (H) *PD-L1* promoter activity in *ARID1A*-ko and sh*NPM1* human TNBC cells measured by dual-luciferase assay. (I) Coculture and cytokine secretion assays using *ARID1A*-ko and sh*NPM1* human TNBC cells as described in Figure 2G. \*\*\**P* < 0.001, ns not significantly different.

Abbreviations: ARID1A, AT-rich interaction domain 1A; *NPM1*, nucleophosmin 1; PD-L1, programmed cell death 1 ligand 1; BRG1, SWI/SNF related, matrix associated, actin dependent regulator of chromatin, subfamily a, member 4; ko, knockout; oe, overexpression; sh, short hairpin RNA-mediated knockdown; nc, negative control; IHC, immunohistochemistry staining; FUSCC, Fudan University Shanghai Cancer Center; TNBC, triple-negative breast cancer; TMA, tissue microarray; ChIP, chromatin immunoprecipitation; ATAC, assay for transposase accessible chromatin; qPCR, quantitative real-time PCR.

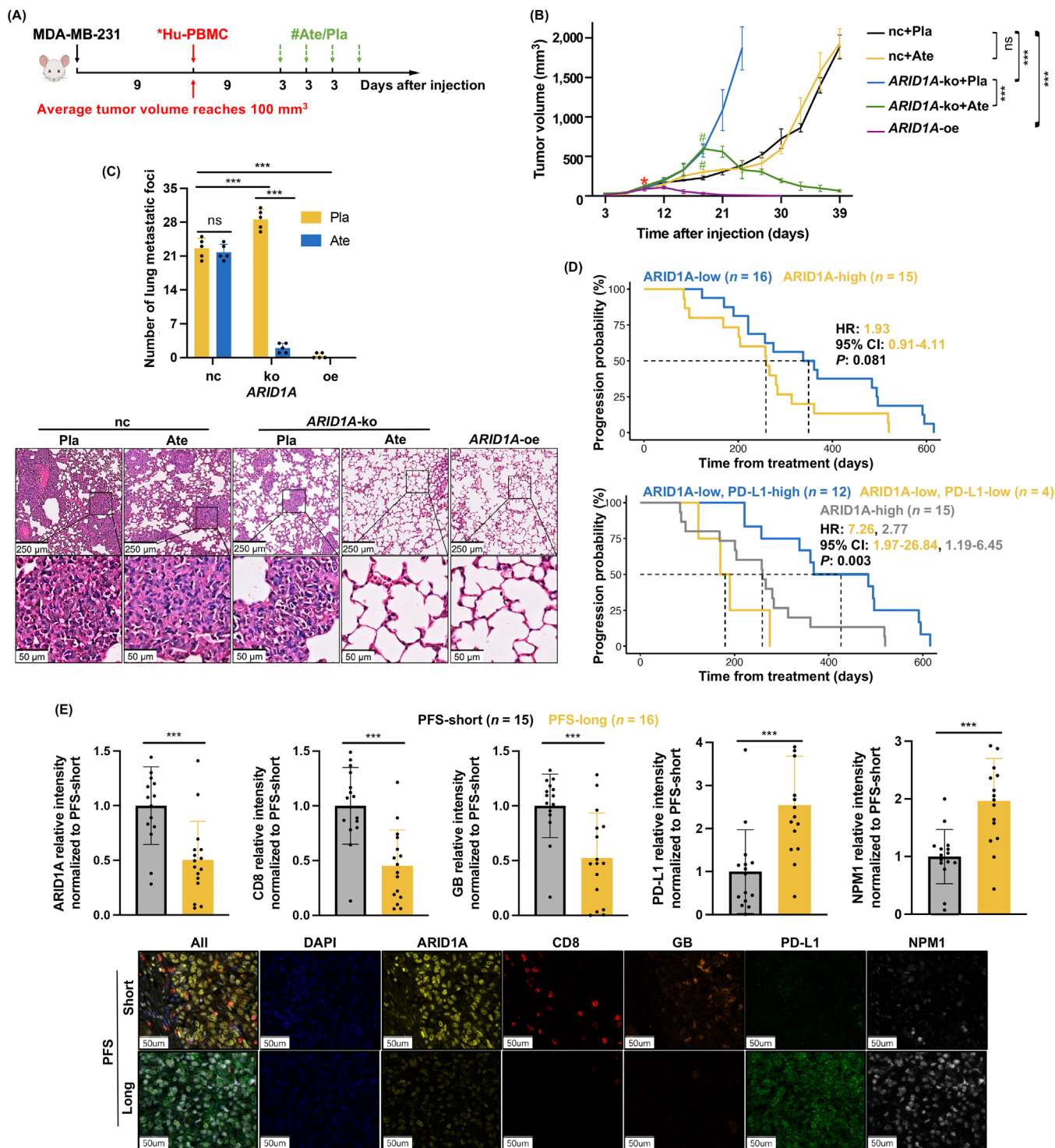


**FIGURE 6** TNBC AIR and PD-L1 contributed by low ARID1A expression could be targeted by ICI. (A) Schematic diagram of the dosage regimen ( $n = 5$  for each group). Black arrow: tumor cell injection. \* Hu-PBMC engraftment when average tumor volume reaches  $100 \text{ mm}^3$  (day 9). # atezolizumab (Ate) or placebo (Pla) administration. (B) Average tumor volume depicted over time. (C) Quantification of lung metastatic foci (up) and representative HE staining (down). (D) Kaplan–Meier analysis for PFS based on ARID1A and PD-L1 expression in CTR20191353. (E) Quantification (up) and representative multispectral fluorescent IHC (down) of ARID1A, CD8<sup>+</sup> T cell markers, PD-L1 and NPM1 by PFS in CTR20191353. \*\*\* $P < 0.001$ , ns not significantly different.

Abbreviations: TNBC, triple-negative breast cancer; AIR, adaptive immune resistance; PD-L1, programmed cell death 1 ligand 1; ARID1A, AT-rich interaction domain 1A; ICI, immune checkpoint inhibitor; Hu-PBMC, human peripheral blood mononuclear cell; HE, hematoxylin-eosin; PFS, progression-free survival; IHC, immunohistochemistry staining; NPM1, nucleophosmin 1; GB, granzyme B; ko, knockout; oe, overexpression; nc, negative control.

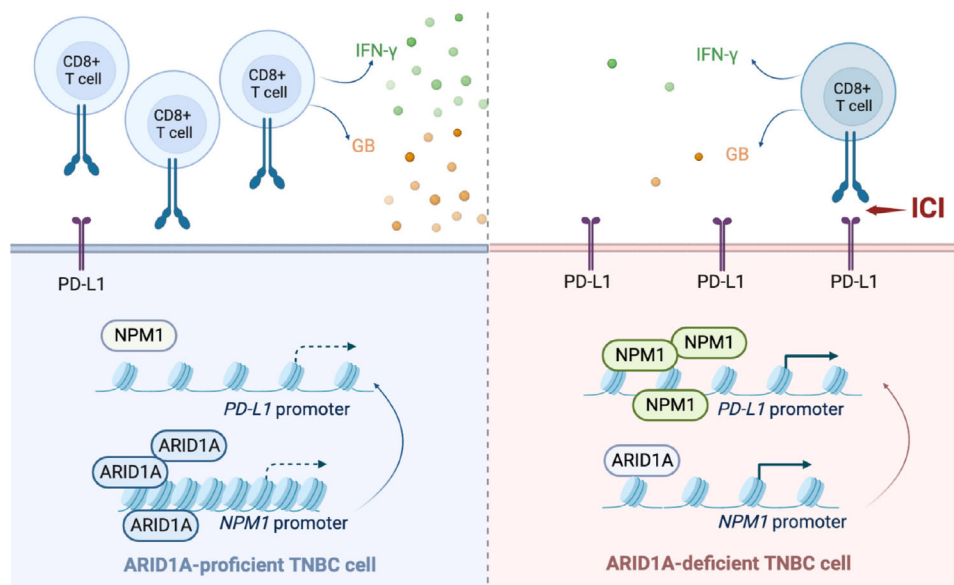


**FIGURE 7** Schematic diagram of the working model.

Abbreviations: TNBC, triple-negative breast cancer; ARID1A, AT-rich interaction domain 1A; NPM1, nucleophosmin 1; PD-L1, programmed cell death 1 ligand 1; IFN- $\gamma$ , interferon; GB, granzyme B; ICI, immune checkpoint inhibitor.

counterparts. Therefore, we propose that although low ARID1A expression provided survival advantage for TNBC cells, it simultaneously left the Achilles' heel, which could be targeted with ICI. This phenomenon was similar to that of patients with human epidermal growth factor receptor 2 (HER2)-positive breast cancer. Although characterized by poorer survival compared with HER2- counterparts, HER2+ patients could profoundly benefit from HER2-targeted treatment and showed better survival [54–56].

It is widely accepted that immune responses triggered by tumor antigens participate in tumor clearance. However, the execution and restimulation of this response are often impaired in cancer through AIR, further limiting effective anti-tumor immunity and leading to continued tumor progression [57]. PD-L1 expression induced by IFN- $\gamma$  is the most classical mechanism for AIR induction [58]. In the present study, we observed a negative correlation between ARID1A and PD-L1 expression in primary and metastatic TNBC. This is consistent with findings in ovarian [12], gastric [59] and colorectal cancers [60], but the underlying mechanism remained open for discussion. In gastric cancer, for instance, ARID1A loss promoted PD-L1 through the phosphatidylinositol 3-kinase (PI3K)/protein kinase B (AKT) pathway [59]. Other regulatory mechanisms for TIME components have also been reported. In prostate cancer, ARID1A loss decreased infiltration of total T cells and IFN- $\gamma$ <sup>+</sup>CD8<sup>+</sup> T cells in TIME through recruiting myeloid-derived suppressor cells, leading to an inhibitory microenvironment and disease progression [61]. In the present study, we also found low ARID1A expres-

sion in TNBC was associated with reduced CD8<sup>+</sup> T cell infiltration and inactivation. Our results further expanded the understanding of ARID1A-mediated TIME regulation in TNBC and provided mechanistic evidence for new treatment strategies.

As a well-established chromatin remodeler, ARID1A exerted bilateral regulation on chromatin accessibility. Schick et al. [62] characterized a panel of isogenic HAP1 cell lines with individual knockouts of 22 BAF subunits, including *ARID1A*. ATAC-seq in *ARID1A*-ko and negative control cells revealed that although the proportion of regions with reduced accessibility was approximately 4.5 times that of regions with increased accessibility, both tendencies existed. In addition, they also showed that gene transcriptomic changes was associated with altered chromatin accessibility [62]. Similar cases have also been reported in colorectal cancer HCT116 cells where *ARID1A*-ko led to increased accessibility at 1.9% sites and decreased accessibility at 6.8% sites (fold change: 3.6) compared with control cells [63]. However, ARID1A deficiency in lung tumors significantly increased global ATAC peaks, indicating an overall elevation in chromatin accessibility [64]. In the present study, ATAC-seq showed that *ARID1A*-ko in MDA-MB-231 cells significantly increased chromatin accessibility at 109,858 sites while 37,668 sites showed significantly decreased chromatin accessibility. Also, pathway enrichment analysis of ATAC-seq showed that AIR-related pathways were enriched in *ARID1A*-ko cells compared with negative control. In the context of the above global variations, low ARID1A expression-promoted

*NPM1* chromatin accessibility increase and subsequent PD-L1 elevation played a pivotal role in AIR in TNBC. Still, further study is needed to explore why *NPM1*, in particular, increases chromatin accessibility upon *ARID1A*-ko.

*NPM1* demonstrated a high mutation rate in hematological diseases, and high *NPM1* expression has been reported in solid tumors such as gastric, thyroid and liver cancers, further regulating DNA replication and transcription [65]. Specifically, *NPM1* has been shown to directly bind to the G-rich repetitive sequence TTAGGG in the *PD-L1* promoter to endogenously activate its transcription in TNBC [66]. In the present study, we observed enrichment of the *NPM1* neighborhood in *ARID1A*-ko MDA-MB-231 cells relative to negative control. For GSEA, neighborhood sets are defined by expression neighborhoods centered on 380 cancer-related genes [43]. Eukaryotic chromosomes could be organized into territories spanning several megabases, and the physical interactions between different genomic segments resulted in chromosomal loops and bridges, contributing to the transcriptional silencing and activation of genes within the three-dimensional context of the nuclear architecture [67]. As a chromatin remodeler, therefore, *ARID1A* may alter gene expression by influencing the entire neighborhood. Our finding that the *NPM1* neighborhood was enriched upon *ARID1A*-ko further supported that *ARID1A* may directly bind to *NPM1* to remodel this chromatin region.

One of the major barriers of ICI treatment is that only a minority of advanced/metastatic TNBC patients demonstrated response [5–7]. Therefore, it is of vital importance to identify those who are likely to benefit from ICI treatment. Our study pinpointed low *ARID1A* expression in TNBC as a novel biomarker for ICIs such as Ate and pucotenlimab from the epigenetic perspective. *ARID1A* deficiency-induced AIR, as well as PD-L1 expression elevation, could be targeted in both xenograft models and patients through Ate and pucotenlimab, respectively. Previous studies in ovarian [12] and lung cancers [68] also found *ARID1A* deficiency to be associated with better ICI treatment effects compared with *ARID1A*-proficient tumors. Therefore, low *ARID1A* expression demonstrated the potential to be a universal marker.

Although being an approved marker for ICI efficacy, PD-L1 positivity still demonstrated limited predictive value due to heterogeneity [69, 70]. Patients bearing a constitutive expression of PD-L1 induced by genetic alterations, such as phosphatase and tensin homolog (*PTEN*) deletions, phosphatidylinositol-4,5-bisphosphate 3-kinase catalytic subunit alpha (*PIK3CA*) and/or *AKT* mutations, epidermal growth factor receptor (*EGFR*) mutations and *MYC* overexpression, failed to respond to ICIs in the absence of immune infiltration [71–73]. The Future-C-Plus trial showed that metastatic TNBC patients with CD8 and/or

PD-L1 positivity benefited more from the PD-1 monoclonal antibody camrelizumab relative to CD8/PD-L1 double negative patients [74]. Based on the classical AIR theory, ICIs should be effective in type II AIR manifested by both PD-L1-positive tumor cells and PD-1-positive T cells, especially CD8<sup>+</sup> T cells [57]. On the contrary, our results showed that TNBC with low *ARID1A* and high PD-L1 expression demonstrated better response to anti-PD-1/PD-L1 therapy Ate and pucotenlimab relative to *ARID1A*-high TNBC in clinical trials and mouse models despite insufficient anti-tumor immune infiltrates, especially CD8<sup>+</sup> T cells. The exciting finding implied that among TNBC with deficient CD8<sup>+</sup> T cell infiltration, previously not considered candidates for ICIs, there existed an immunological subgroup characterized by low *ARID1A* and high PD-L1 expression that could benefit from ICIs.

One limitation of our research is the failure to demonstrate reciprocal interactions between immune cells and metastatic TNBC cells harboring *ARID1A* deficiency. There is an ethical issue here, and it remained difficult to distinguish *ARID1A*-related AIR from AIR induced by other causes. Nevertheless, further research on tumor-immune coevolution in TNBC is ongoing to reverse low *ARID1A* expression-promoted AIR.

## 5 | CONCLUSIONS

Our study identified low expression of the epigenetic modulator *ARID1A* in TNBC as a novel subtype of AIR through increasing *NPM1* chromatin accessibility and subsequent *PD-L1* transcription. This immunological subgroup of TNBC defined by low *ARID1A* and further characterized by high PD-L1 expression could potentially benefit from ICI.

## DECLARATIONS

### AUTHOR CONTRIBUTIONS

ZHT, XCH and XYC outlined the manuscript. ZHT, XCH, JZ, BYW and ZMS contributed to the preparation of clinical data. ZHT, XYC, TN and SLH performed literature search. XYC, BL, TN, YY, LHH, YW, JJ and MDY contributed to data collection, analysis and interpretation. ZHT, XYC and BL provided the figures and drafted the manuscript, with additional input from all authors. ZHT, XCH, TN, SLH and XYC contributed to manuscript review and editing. All authors read and approved the final manuscript.

## ACKNOWLEDGMENTS

We are grateful to all members of the Department of Breast and Urologic Medical Oncology in FUSCC for helping to complete this project. This work was supported by

the National Science and Technology Major Project (grant number: 2020ZX09201-013 to XCH).

## CONFLICT OF INTEREST STATEMENT

The authors declare no conflict of interest.

## ETHICS APPROVAL AND CONSENT TO PARTICIPATE

All research protocols were approved by the medical ethics committee of Fudan University Shanghai Cancer Center (050432-4-2108\*). Written informed consent was obtained from all patients.

## CONSENT FOR PUBLICATION

Not applicable.

## DATA AVAILABILITY STATEMENT

RNA-seq, ChIP-seq and ATAC-seq data have been deposited to the GEO repository with the accession number GSE234179. Other datasets generated or analyzed during the current study are available in TCGA Program (<https://www.cbioportal.org>), UCSC Genome Browser (<https://genome.ucsc.edu>), GEO repository (<https://www.ncbi.nlm.nih.gov/geo/>), Molecular Signature Database (<https://www.gsea-msigdb.org/gsea/msigdb/index.jsp>), Gene Ontology Resource (<http://geneontology.org>), EnhancerDB (<http://lcbw.swjtu.edu.cn/EnhancerDB/>) and PubMed (<https://pubmed.ncbi.nlm.nih.gov>).

## ORCID

Bi-Yun Wang  <https://orcid.org/0000-0002-7829-1544>

Xi-Chun Hu  <https://orcid.org/0000-0001-6148-9186>

Zhong-Hua Tao  <https://orcid.org/0000-0003-3975-3803>

## REFERENCES

1. Lei S, Zheng R, Zhang S, Wang S, Chen R, Sun K, et al. Global patterns of breast cancer incidence and mortality: A population-based cancer registry data analysis from 2000 to 2020. *Cancer Commun (Lond)*. 2021;41(11):1183–94.
2. Savas P, Salgado R, Denkert C, Sotiriou C, Darcy PK, Smyth MJ, et al. Clinical relevance of host immunity in breast cancer: from TILs to the clinic. *Nat Rev Clin Oncol*. 2016;13(4):228–41.
3. Bareche Y, Buisseret L, Gruosso T, Girard E, Venet D, Dupont F, et al. Unraveling Triple-Negative Breast Cancer Tumor Microenvironment Heterogeneity: Towards an Optimized Treatment Approach. *J Natl Cancer Inst*. 2020;112(7):708–19.
4. Cortes J, Cescon DW, Rugo HS, Nowecki Z, Im SA, Yusof MM, et al. Pembrolizumab plus chemotherapy versus placebo plus chemotherapy for previously untreated locally recurrent inoperable or metastatic triple-negative breast cancer (KEYNOTE-355): a randomised, placebo-controlled, double-blind, phase 3 clinical trial. *Lancet*. 2020;396(10265):1817–28.
5. Winer EP, Lipatov O, Im SA, Goncalves A, Munoz-Couselo E, Lee KS, et al. Pembrolizumab versus investigator-choice chemotherapy for metastatic triple-negative breast cancer (KEYNOTE-119): a randomised, open-label, phase 3 trial. *Lancet Oncol*. 2021;22(4):499–511.
6. Adams S, Diamond JR, Hamilton E, Pohlmann PR, Tolaney SM, Chang CW, et al. Atezolizumab Plus nab-Paclitaxel in the Treatment of Metastatic Triple-Negative Breast Cancer With 2-Year Survival Follow-up: A Phase 1b Clinical Trial. *JAMA Oncol*. 2019;5(3):334–42.
7. Adams S, Schmid P, Rugo HS, Winer EP, Loirat D, Awada A, et al. Pembrolizumab monotherapy for previously treated metastatic triple-negative breast cancer: cohort A of the phase II KEYNOTE-086 study. *Ann Oncol*. 2019;30(3):397–404.
8. Aftimos P, Oliveira M, Irrthum A, Fumagalli D, Sotiriou C, Gal-Yam EN, et al. Genomic and Transcriptomic Analyses of Breast Cancer Primaries and Matched Metastases in AURORA, the Breast International Group (BIG) Molecular Screening Initiative. *Cancer Discov*. 2021;11(11):2796–811.
9. Ma H, Kang Z, Foo TK, Shen Z, Xia B. Disrupted BRCA1-PALB2 interaction induces tumor immunosuppression and T-lymphocyte infiltration in HCC through cGAS-STING pathway. *Hepatology*. 2022;77(1):33–47.
10. Ma S, Zhao Y, Lee WC, Ong LT, Lee PL, Jiang Z, et al. Hypoxia induces HIF1alpha-dependent epigenetic vulnerability in triple negative breast cancer to confer immune effector dysfunction and resistance to anti-PD-1 immunotherapy. *Nat Commun*. 2022 Jul 15;13(1):4118.
11. Lai Q, Wang H, Li A, Xu Y, Tang L, Chen Q, et al. Decitabine improve the efficiency of anti-PD-1 therapy via activating the response to IFN/PD-L1 signal of lung cancer cells. *Oncogene*. 2018;37(17):2302–12.
12. Shen J, Ju Z, Zhao W, Wang L, Peng Y, Ge Z, et al. ARID1A deficiency promotes mutability and potentiates therapeutic anti-tumor immunity unleashed by immune checkpoint blockade. *Nat Med*. 2018;24(5):556–62.
13. Braun DA, Ishii Y, Walsh AM, Van Allen EM, Wu CJ, Shukla SA, et al. Clinical Validation of PBRM1 Alterations as a Marker of Immune Checkpoint Inhibitor Response in Renal Cell Carcinoma. *JAMA Oncol*. 2019;5(11):1631–33.
14. Goswami S, Chen Y, Anandhan S, Szabo PM, Basu S, Blando JM, et al. ARID1A mutation plus CXCL13 expression act as combinatorial biomarkers to predict responses to immune checkpoint therapy in mUCC. *Sci Transl Med*. 2020;12(548).
15. Wu JI, Lessard J, Crabtree GR. Understanding the words of chromatin regulation. *Cell*. 2009;136(2):200–6.
16. Wilson BG, Roberts CW. SWI/SNF nucleosome remodellers and cancer. *Nat Rev Cancer*. 2011;11(7):481–92.
17. Nagarajan S, Rao SV, Sutton J, Cheeseman D, Dunn S, Papachristou EK, et al. ARID1A influences HDAC1/BRD4 activity, intrinsic proliferative capacity and breast cancer treatment response. *Nat Genet*. 2020;52(2):187–97.
18. Xu G, Chhangawala S, Cocco E, Razavi P, Cai Y, Otto JE, et al. ARID1A determines luminal identity and therapeutic response in estrogen-receptor-positive breast cancer. *Nat Genet*. 2020;52(2):198–207.
19. Bitler BG, Fatkhutdinov N, Zhang R. Potential therapeutic targets in ARID1A-mutated cancers. *Expert Opin Ther Targets*. 2015;19(11):1419–22.

20. Jiang T, Chen X, Su C, Ren S, Zhou C. Pan-cancer analysis of ARID1A Alterations as Biomarkers for Immunotherapy Outcomes. *J Cancer*. 2020;11(4):776–80.
21. Sun X, Wang SC, Wei Y, Luo X, Jia Y, Li L, et al. Arid1a Has Context-Dependent Oncogenic and Tumor Suppressor Functions in Liver Cancer. *Cancer Cell*. 2017;32(5):574–89 e6.
22. Fontana B, Gallerani G, Salamon I, Pace I, Roncarati R, Ferracin M. ARID1A in cancer: Friend or foe? *Front Oncol*. 2023;13:1136248.
23. Tao Z, Li T, Feng Z, Liu C, Shao Y, Zhu M, et al. Characterizations of Cancer Gene Mutations in Chinese Metastatic Breast Cancer Patients. *Front Oncol*. 2020;10:1023.
24. Jiang YZ, Ma D, Suo C, Shi J, Xue M, Hu X, et al. Genomic and Transcriptomic Landscape of Triple-Negative Breast Cancers: Subtypes and Treatment Strategies. *Cancer Cell*. 2019;35(3):428–40 e5.
25. Yates LR, Knappskog S, Wedge D, Farmery JHR, Gonzalez S, Martincorena I, et al. Genomic Evolution of Breast Cancer Metastasis and Relapse. *Cancer Cell*. 2017;32(2):169–84 e7.
26. Li CW, Lim SO, Xia W, Lee HH, Chan LC, Kuo CW, et al. Glycosylation and stabilization of programmed death ligand-1 suppresses T-cell activity. *Nat Commun*. 2016;7:12632.
27. Burr ML, Sparbier CE, Chan YC, Williamson JC, Woods K, Beavis PA, et al. CMTM6 maintains the expression of PD-L1 and regulates anti-tumour immunity. *Nature*. 2017;549(7670):101–05.
28. Hui E, Cheung J, Zhu J, Su X, Taylor MJ, Wallweber HA, et al. T cell costimulatory receptor CD28 is a primary target for PD-1-mediated inhibition. *Science*. 2017;355(6332):1428–33.
29. Zhang Q, Zhang Y, Chen Y, Qian J, Zhang X, Yu K. A Novel mTORC1/2 Inhibitor (MTI-31) Inhibits Tumor Growth, Epithelial-Mesenchymal Transition, Metastases, and Improves Antitumor Immunity in Preclinical Models of Lung Cancer. *Clin Cancer Res*. 2019;25(12):3630–42.
30. Langmead B, Salzberg SL. Fast gapped-read alignment with Bowtie 2. *Nat Methods*. 2012 Mar 4;9(4):357–9.
31. Zhang Y, Liu T, Meyer CA, Eeckhoutte J, Johnson DS, Bernstein BE, et al. Model-based analysis of ChIP-Seq (MACS). *Genome Biol*. 2008;9(9):R137.
32. Shen L, Shao NY, Liu X, Maze I, Feng J, Nestler EJ. diffReps: detecting differential chromatin modification sites from ChIP-seq data with biological replicates. *PLoS One*. 2013;8(6):e65598.
33. Buenrostro JD, Wu B, Chang HY, Greenleaf WJ. ATAC-seq: A Method for Assaying Chromatin Accessibility Genome-Wide. *Curr Protoc Mol Biol*. 2015;109:21 29 1–21 29 9.
34. Zhang P, Liu Y, Lian C, Cao X, Wang Y, Li X, et al. SH3RF3 promotes breast cancer stem-like properties via JNK activation and PTX3 upregulation. *Nat Commun*. 2020;11(1):2487.
35. Lin S, Huang G, Cheng L, Li Z, Xiao Y, Deng Q, et al. Establishment of peripheral blood mononuclear cell-derived humanized lung cancer mouse models for studying efficacy of PD-L1/PD-1 targeted immunotherapy. *MAbs*. 2018;10(8):1301–11.
36. Hammond ME, Hayes DF, Dowsett M, Allred DC, Hagerty KL, Badve S, et al. American Society of Clinical Oncology/College Of American Pathologists guideline recommendations for immunohistochemical testing of estrogen and progesterone receptors in breast cancer. *J Clin Oncol*. 2010;28(16):2784–95.
37. Wolff AC, Hammond MEH, Allison KH, Harvey BE, Mangu PB, Bartlett JMS, et al. Human Epidermal Growth Factor Receptor 2 Testing in Breast Cancer: American Society of Clinical Oncology/College of American Pathologists Clinical Practice Guideline Focused Update. *J Clin Oncol*. 2018;36(20):2105–22.
38. Amin MB, Greene FL, Edge SB, Compton CC, Gershenwald JE, Brookland RK, et al. The Eighth Edition AJCC Cancer Staging Manual: Continuing to build a bridge from a population-based to a more “personalized” approach to cancer staging. *CA Cancer J Clin*. 2017;67(2):93–99.
39. Giuliano AE, Edge SB, Hortobagyi GN. Eighth Edition of the AJCC Cancer Staging Manual: Breast Cancer. *Ann Surg Oncol*. 2018;25(7):1783–85.
40. Cao J, Wang B, Zhang J, Tao Z, Wang L, Hu X. Phase 1b clinical trial of pucotenlimab (HX008), a novel anti-PD-1 monoclonal antibody, combined with gemcitabine and cisplatin in the first-line treatment of metastatic triple-negative breast cancer. *Front Oncol*. 2022;12:837963.
41. Guo H, Ding Q, Gong Y, Gilcrease MZ, Zhao M, Zhao J, et al. Comparison of three scoring methods using the FDA-approved 22C3 immunohistochemistry assay to evaluate PD-L1 expression in breast cancer and their association with clinicopathologic factors. *Breast Cancer Res*. 2020;22(1):69.
42. Ikarashi D, Kitano S, Tsuyukubo T, Takenouchi K, Nakayama T, Onagi H, et al. Pretreatment tumour immune microenvironment predicts clinical response and prognosis of muscle-invasive bladder cancer in the neoadjuvant chemotherapy setting. *Br J Cancer*. 2022;126(4):606–14.
43. Subramanian A, Tamayo P, Mootha VK, Mukherjee S, Ebert BL, Gillette MA, et al. Gene set enrichment analysis: a knowledge-based approach for interpreting genome-wide expression profiles. *Proc Natl Acad Sci U S A*. 2005;102(43):15545–50.
44. Liberzon A, Subramanian A, Pinchback R, Thorvaldsdottir H, Tamayo P, Mesirov JP. Molecular signatures database (MSigDB) 3.0. *Bioinformatics*. 2011;27(12):1739–40.
45. Ayers M, Lunceford J, Nebozhyn M, Murphy E, Loboda A, Kaufman DR, et al. IFN-gamma-related mRNA profile predicts clinical response to PD-1 blockade. *J Clin Invest*. 2017;127(8):2930–40.
46. Qin Y, Ekmekcioglu S, Forget MA, Szekvolgyi L, Hwu P, Grimm EA, et al. Cervical Cancer Neoantigen Landscape and Immune Activity is Associated with Human Papillomavirus Master Regulators. *Front Immunol*. 2017;8:689.
47. Yim SY, Kang SH, Shin JH, Jeong YS, Sohn BH, Um SH, et al. Low ARID1A Expression is Associated with Poor Prognosis in Hepatocellular Carcinoma. *Cells*. 2020;9(9):2002
48. Mehrvarz Sarshekeh A, Alshenaifi J, Roszik J, Manyam GC, Advani SM, Katkhuda R, et al. ARID1A Mutation May Define an Immunologically Active Subgroup in Patients with Microsatellite Stable Colorectal Cancer. *Clin Cancer Res*. 2021;27(6):1663–70.
49. Colaprico A, Silva TC, Olsen C, Garofano L, Cava C, Garolini D, et al. TCGAAbiolinks: an R/Bioconductor package for integrative analysis of TCGA data. *Nucleic Acids Res*. 2016;44(8):e71.
50. Chen B, Khodadoust MS, Liu CL, Newman AM, Alizadeh AA. Profiling Tumor Infiltrating Immune Cells with CIBERSORT. *Methods Mol Biol*. 2018;1711:243–59.
51. Thorsson V, Gibbs DL, Brown SD, Wolf D, Bortone DS, Ou Yang TH, et al. The Immune Landscape of Cancer. *Immunity*. 2018;48(4):812–30 e14.

52. Li T, Fan J, Wang B, Traugh N, Chen Q, Liu JS, et al. TIMER: A Web Server for Comprehensive Analysis of Tumor-Infiltrating Immune Cells. *Cancer Res.* 2017;77(21):e108–e10.
53. Picelli S, Faridani OR, Bjorklund AK, Winberg G, Sagasser S, Sandberg R. Full-length RNA-seq from single cells using Smart-seq2. *Nat Protoc.* 2014;9(1):171–81.
54. Slamon DJ, Leyland-Jones B, Shak S, Fuchs H, Paton V, Bajamonde A, et al. Use of chemotherapy plus a monoclonal antibody against HER2 for metastatic breast cancer that over-expresses HER2. *N Engl J Med.* 2001;344(11):783–92.
55. Burstein HJ. The distinctive nature of HER2-positive breast cancers. *N Engl J Med.* 2005;353(16):1652–4.
56. Cameron D, Piccart-Gebhart MJ, Gelber RD, Procter M, Goldhirsch A, de Azambuja E, et al. 11 years' follow-up of trastuzumab after adjuvant chemotherapy in HER2-positive early breast cancer: final analysis of the HERceptin Adjuvant (HERA) trial. *Lancet.* 2017;389(10075):1195–205.
57. Kim TK, Vandsemb EN, Herbst RS, Chen L. Adaptive immune resistance at the tumour site: mechanisms and therapeutic opportunities. *Nat Rev Drug Discov.* 2022;21(7):529–40.
58. Freeman GJ, Long AJ, Iwai Y, Bourque K, Chernova T, Nishimura H, et al. Engagement of the PD-1 immunoinhibitory receptor by a novel B7 family member leads to negative regulation of lymphocyte activation. *J Exp Med.* 2000;192(7):1027–34.
59. Kim YB, Ahn JM, Bae WJ, Sung CO, Lee D. Functional loss of ARID1A is tightly associated with high PD-L1 expression in gastric cancer. *Int J Cancer.* 2019;145(4):916–26.
60. Kamori T, Oki E, Shimada Y, Hu Q, Hisamatsu Y, Ando K, et al. The effects of ARID1A mutations on colorectal cancer and associations with PD-L1 expression by stromal cells. *Cancer Rep (Hoboken).* 2022;5(1):e1420.
61. Li N, Liu Q, Han Y, Pei S, Cheng B, Xu J, et al. ARID1A loss induces polymorphonuclear myeloid-derived suppressor cell chemotaxis and promotes prostate cancer progression. *Nat Commun.* 2022;13(1):7281.
62. Schick S, Rendeiro AF, Runggatscher K, Ringler A, Boidol B, Hinkel M, et al. Systematic characterization of BAF mutations provides insights into intracomplex synthetic lethality in human cancers. *Nat Genet.* 2019;51(9):1399–410.
63. Kelso TWR, Porter DK, Amaral ML, Shokhirev MN, Benner C, Hargreaves DC. Chromatin accessibility underlies synthetic lethality of SWI/SNF subunits in ARID1A-mutant cancers. *Elife.* 2017;6.
64. Liu X, Li Z, Wang Z, Liu F, Zhang L, Ke J, et al. Chromatin Remodeling Induced by ARID1A Loss in Lung Cancer Promotes Glycolysis and Confers JQ1 Vulnerability. *Cancer Res.* 2022;82(5):791–804.
65. Box JK, Paquet N, Adams MN, Boucher D, Bolderson E, O'Byrne KJ, et al. Nucleophosmin: from structure and function to disease development. *BMC Mol Biol.* 2016;17(1):19.
66. Qin G, Wang X, Ye S, Li Y, Chen M, Wang S, et al. NPM1 upregulates the transcription of PD-L1 and suppresses T cell activity in triple-negative breast cancer. *Nat Commun.* 2020;11(1):1669.
67. De S, Babu MM. Genomic neighbourhood and the regulation of gene expression. *Curr Opin Cell Biol.* 2010;22(3):326–33.
68. Lee JB, Park HS, Choi SJ, Heo SG, An HJ, Kim HR, et al. Plasma tumor mutation burden is associated with clinical benefit in patients with non-small cell lung cancer treated with anti-programmed death-1 monotherapy. *Ther Adv Med Oncol.* 2022;14:17588359221141761.
69. Wilke CM, Wei S, Wang L, Kryczek I, Kao J, Zou W. Dual biological effects of the cytokines interleukin-10 and interferon-gamma. *Cancer Immunol Immunother.* 2011;60(11):152figure–41.
70. Gao Y, Yang J, Cai Y, Fu S, Zhang N, Fu X, et al. IFN-gamma-mediated inhibition of lung cancer correlates with PD-L1 expression and is regulated by PI3K-AKT signaling. *Int J Cancer.* 2018;143(4):931–43.
71. Parsa AT, Waldron JS, Panner A, Crane CA, Parney IF, Barry JJ, et al. Loss of tumor suppressor PTEN function increases B7-H1 expression and immunoresistance in glioma. *Nat Med.* 2007;13(1):84–8.
72. Casey SC, Tong L, Li Y, Do R, Walz S, Fitzgerald KN, et al. MYC regulates the antitumor immune response through CD47 and PD-L1. *Science.* 2016;352(6282):227–31.
73. Dorand RD, Nthale J, Myers JT, Barkauskas DS, Avril S, Chirieleison SM, et al. Cdk5 disruption attenuates tumor PD-L1 expression and promotes antitumor immunity. *Science.* 2016;353(6297):399–403.
74. Wu SY, Xu Y, Chen L, Fan L, Ma XY, Zhao S, et al. Combined angiogenesis and PD-1 inhibition for immunomodulatory TNBC: concept exploration and biomarker analysis in the FUTURE-C-Plus trial. *Mol Cancer.* 2022;21(1):84.

## SUPPORTING INFORMATION

Additional supporting information can be found online in the Supporting Information section at the end of this article.

**How to cite this article:** Chen X-Y, Li B, Wang Y, Jin J, Yang Y, Huang L-H, et al. Low level of ARID1A contributes to adaptive immune resistance and sensitizes triple-negative breast cancer to immune checkpoint inhibitors. *Cancer Commun.* 2023;1–24. <https://doi.org/10.1002/cac2.12465>